IDŐJÁRÁS

QUARTERLY JOURNAL
OF THE HUNGARIAN METEOROLOGICAL SERVICE

CONTENTS

Judit Kerényi and *Mária Putsay:* Extreme flood monitoring in Romania and Hungary using Earth Observation Data 205

Zsuzsanna Dezső, Judit Bartholy and *Rita Pongrácz:* Satellite-based analysis of the urban heat island effect..... 217

Steluţa Vasiliu and *András Horányi:* An evaluation of the performance of the three-dimensional variational data assimilation scheme for the ALADIN/HU spectral limited area model..... 233

Dezső Szepesi, Katalin Fekete, Richárd Büki, László Koncsos and *Endre Kovács:* Development of regulatory transmission modeling in Hungary..... 257

Book review..... 281

****

http://omsz.met.hu/omsz.php?almenu_id=omsz&pid=references&pri=2

VOL. 109 * NO. 4 * OCTOBER – DECEMBER 2005

IDŐJÁRÁS

Quarterly Journal of the Hungarian Meteorological Service

Editorial Office: P.O. Box 39, H-1675 Budapest, Hungary or
Gilice tér 39, H-1181 Budapest, Hungary
E-mail: bozo.l@met.hu or *antal.e@met.hu*
Fax: (36-1) 346-4809

Subscription by

mail: IDŐJÁRÁS, P.O. Box 39, H-1675 Budapest, Hungary;
E-mail: bozo.l@met.hu or *antal.e@met.hu*; *Fax: (36-1) 346-4809*

IDŐJÁRÁS

Quarterly Journal of the Hungarian Meteorological Service
Vol. 109, No. 4, October–December 2005, pp. 205–216

Extreme flood monitoring in Romania and Hungary using Earth Observation Data

Judit Kerényi and **Mária Putsay**

Hungarian Meteorological Service
P.O. Box 38, H-1525 Budapest, Hungary; E-mail: kerenyi.j@met.hu

(Manuscript received in final form September 19, 2005)

Abstract—In the recent years, large and extreme floods occurred frequently in many parts of the world. One region, which suffers from flood damages on a regular basis, is the transboundary area of the Fehér-Körös and Fekete-Körös rivers flowing from Romania to Hungary. For further improvement of flood management in this area, an international team was formed. The paper provides a brief overview of the whole project and a more detailed description of the satellite data processing tools elaborated for the project, developed at the Hungarian Meteorological Service (HMS). Both the ASTER and MODIS instruments are flying on the Terra and Aqua satellites. Our tasks were to produce a high-resolution land use map about the study area and to develop a method for floodwater detection. Land use map was used as background information with topographical, physiographical, and hydrological parameters in the GIS database. It was derived by applying 15 m spatial resolution ASTER images. At the water detection, the data of the MODIS instrument were used. This instrument measures in 36 channels and the spatial resolutions of these are 250 m, 500 m, and 1000 m depending on the channel. Two methods were developed for water detection. Both methods are based on threshold techniques. One is automatic, quick, but less accurate, as it may contain misdetected cloud shadow pixels. The other algorithm is a more accurate semi-automatic method, but interactive correction is needed if the investigated area is partly cloudy. Water masks were derived for the days of the flood event in spring of 2000.

Key-words: flood management, remote sensing, land use map, detecting flood water, ASTER, MODIS.

1. Introduction

The cost of natural disasters is increasing; their impact is invariably higher in developing countries and where people are concentrated. Many factors contribute to increasing vulnerability, such as unsustainable development practices,

degradation of natural resources, weak disaster management and forecasting techniques, or inadequate communications and transport infrastructure.

At the same time there are several technological trends that can serve to decrease the vulnerability to disasters. These include: better understanding of hazardous processes, improved analytical methods and communications. The use of modern and appropriate technologies like remote sensing and GIS can lead to the reduction of social and economic impact of natural disasters, and many technologically advanced nations are today investing heavily in such technology for this purpose.

In the recent years, large and extreme floods occurred frequently in many parts of the world. In the last few years several related projects were lunched. For example, the SIREN project, funded by the European Union with the participation of France, Spain, Italy, and Germany (*Rabaute et al.*, 2002), mainly aims at working on "user services" aspects in order to imagine, define, validate specific concepts, and solutions to make the use of Earth observation derived information easier and more effective for potential users (disaster management services, public services at national and local level, environmental agencies).

One region, which suffers from flood damages on a regular basis, is the transboundary area of the Fehér-Körös and Fekete-Körös rivers flowing from Romania into Hungary. Floods in this area typically start in the mountainous terrain of the upper parts of the Transylvanian Basin in Romania and propagate to the plains in Hungary. Recent floods in this area include the two spring 2000 floods, which caused damages in the Romanian territory. In the Hungarian territory, a particularly notable flood occurred in the summer of 1980.

There exists a close co-operation between Romania and Hungary concerning flood defense. The information provided by Romania to Hungary (downstream) is presently based entirely upon ground based data, mainly collected from the non-automatic hydrometeorological stations. Such data are somewhat limited in respect of spatial distribution, temporal resolution, and speed of collection and transmission.

Recognizing the need for further improvement of flood management in this area, an international team was formed, with representatives of Hungary, Romania, and the USA, and a project started on "Monitoring of Extreme Flood Events in Romania and Hungary Using Earth Observation (EO) Data" in the framework of NATO Science for Peace (SfP) Program. The project concerns the region between 46.5–47.5°N and 20.5–22°E.

Success of risk management largely depends on the availability, dissemination, and effective use of timely information. Remote sensing technologies and the numerical hydrological prediction calculations using the traditional means can greatly improve the management of flood hazards. The

SfP project aims to provide such an efficient and powerful flood monitoring tool. A GIS (Geographic Information System) database is organized merging the surface and remote sensing data, to handle them together.

The paper provides a brief overview of the whole project and a more detailed overview of the satellite data processing tools. This work was done at the Satellite Research Laboratory of the Hungarian Meteorological Service (HMS). Our tasks were to produce a high-resolution land use map about the study area and to develop a method for floodwater detection.

2. The project objectives

The main goal of the project is to provide an efficient and powerful flood-monitoring tool based on new MODIS satellite data to the local and river authorities and to other key organizations. A new flood management system is being established, based on hydrological models, GIS technology with hydrological and meteorological database, traditional surface and satellite remote sensing tools. A database, containing EO data, hydrological and meteorological parameters related to significant flood events, was developed and used to test the processing and analytical algorithms, in order to establish an operational methodology for the detection, mapping, and analysis of flooding. The proposed hydrological forecasting model will increase the lead time and thereby provide additional time for implementing the measures needed to protect the human life and property in the study area. This will lead to direct and indirect reduction of economic losses and an earlier flood warning for the Hungarian territory of the Fehér-Körös and Fekete-Körös rivers.

Finally, the project results described here could also help in restoration and rehabilitation of some river sections, which were adversely altered by floods, and also in future analysis and selection of structural flood protection works.

3. Image processing for flood analysis

In the framework of the project, HMS produced land cover/land use map and detected floodwater. In this work medium spatial resolution MODIS and high resolution ASTER images are applied.

3.1 Land use map using ASTER images

To get information about the land cover for the investigated area, a land use map was derived applying ASTER images. This information will be used as

background information with topographical, physiographical, and hydrological parameters in the GIS database.

ASTER is a sensor onboard the Terra (EOS AM) and Aqua (EOS PM) satellites. The ASTER measures in 14 spectral bands. ASTER images were found suitable for producing detailed maps of land cover/land use. The 15 m spatial resolution visible and near infrared bands were used: band 1–0.56 μm, band 2–0.66 μm, and band 3–0.8 μm.

The spectral characteristics of the water, land (bare soil, different types of vegetation: agriculture, forest, meadows) and cloud surfaces in these three bands are quite different, which allow to separate them by classification. Most land surfaces (including bare soil and vegetation) are brighter in band 3 than band 1, but it is not true for water surfaces and clouds. The water is darker in the near infrared than in the visible part of the spectrum. Clouds are similarly bright in both spectral regions. The two visible bands help to separate the different vegetation types.

For the land classification we used the ENVI software. The land use maps were derived from images taken in 2002–2003.

The method for the land cover/land use mapping included two steps: (a) geo-referencing and (b) data classification. For the classification both supervised and unsupervised methods were tested. Following *Pinilla et al.* (2000), we investigated how many iterations were needed in the unsupervised classification. Better results were obtained with the unsupervised classification, in which different numbers of classes and iterations were tested (90 classes and 40 iterations were chosen). At the post-processing the classes were merged into 8 groups: 4 different agriculture areas, forest, water, cloud, shadow. The urban area could not be separated in a discrete class so they had to be classified manually.

The classification was performed for four ASTER images to cover the Hungarian part of the investigated area, and a mosaic land use map was made from them.

The raster type images are vectorized and evaluated for the GIS data base. The land use maps will be utilized for evaluating the damage of the inundation.

3.2 Short description of MODIS images

In 1999 the Terra (EOS-AM), in 2002 the Aqua (EOS-PM) new satellites were lunched. The key instrument flying on both Terra and Aqua satellites is the Moderate Resolution Imaging Spectroradiometer (MODIS). Both Terra and Aqua view the entire Earth's surface every day. For detection of the flooded area, MODIS images were applied. The new satellite data can be applied in

several other fields of meteorology. For example, in the EUMETSAT Hydrology SAF (http://www.eumetsat.int/en/area4/saf/Internet/ain_safs/hwm/NEW-HSFWG2-SunmmaryReport-rev23-FINAL.html), MODIS data will be used for precipitation estimation, snow detection, surface moisture calculation. MODIS is a passive imaging spectroradiometer, acquiring data in 36 spectral bands. Spatial resolution of the images is 250 m (bands 1–2), 500 m (bands 3–7), and 1000 m (bands 8–36), respectively.

Fig. 1 shows a MODIS visible image received on April 21, 2001, which covers the middle part of Europe. As we can see in *Table 1,* several parameters for land, ocean, and atmosphere in good spatial resolution can be derived.

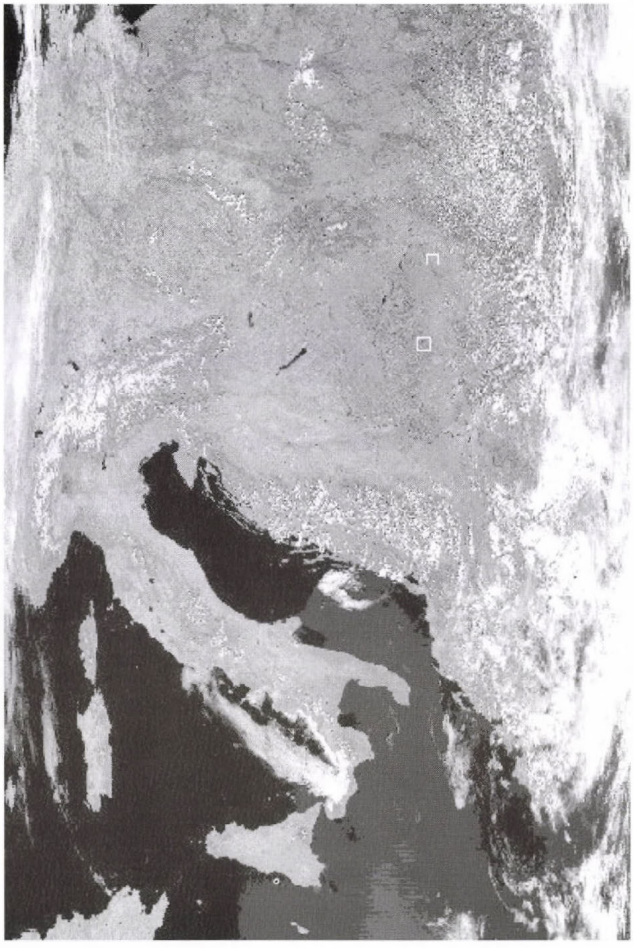

Fig. 1. A TERRA/MODIS image (channel 2) taken on April 21, 2001.

Table 1. Information about the MODIS instrument

Primary use	Bands	Bandwidth
Land/cloud boundaries	1	620–670 nm
	2	841–876 nm
Land/cloud properties	3	459–479 nm
	4	545–565 nm
	5	1230–1250 nm
	6	1628–1652 nm
	7	2105–2155 nm
Ocean color/phytoplankton/ biogeochemistry	8	405–420 nm
	9	438–448 nm
	10	483–493 nm
	11	526–536 nm
	12	546–556 nm
	13	662–762 nm
	14	673–683 nm
	15	743–753 nm
	16	862–877 nm
Atmospheric water vapor	17	890–920 nm
	18	931–941 nm
	19	915–965 nm
Surface/cloud temperature	20	3.660–3.840 μm
	21	3.929–3.989 μm
	22	3.929–3.989 μm
	23	4.020–4.080 μm
Atmospheric temperature	24	4.433–4.498 μm
	25	4.482–4.549 μm
Cirrus clouds	26	1.360–1.390 μm
Water vapor	27	6.535–6.895 μm
	28	7.175–7.475 μm
	29	8.400–8.700 μm
Ozone	30	9.580–9.880 μm
Surface/cloud temperature	31	10.780–11.280 μm
	32	11.770–12.770 μm
Cloud top altitude	33	13.185–13.485 μm
	34	13.485–13.785 μm
	35	13.785–14.085 μm
	36	14.085–14.385 μm

The data available from MODIS are suitable for many different tasks concerning water surfaces, for example investigation of ocean color, water quality monitoring (*Guangyu*, 2005), to detect land cover changes such as

floods, deforestation and burnt scars (*Zhan et al.*, 2002), or flooded area detection (*Kameyama et al.*, 2003).

3.3 Water detection using MODIS data

The MODIS data are highly suitable for flood warning and management, as well, because they are available in real time (or nearly real time), can be rapidly processed and disseminated, cover a wide area, and are abundant and inexpensive, which is important when dealing with longer duration floods. MODIS provides very accurate geo-coding, clouds can be removed by composition techniques, and the data are distributed via the EOS Gateway.

TERRA/MODIS satellite data were used to determine the flood-prone areas. For our purpose we used Level 1B data, channel 1 (0.66 μm) and 2 (0.87 μm) with 250 m spatial resolution, and channel 3 (1.6 μm) with 500 m spatial resolution. The MODIS Level 1B data from the Terra Satellite were downloaded from the EOS Data Gateway, Land Processes Distributed Active Archive Center (LP DAAC) World-Wide Web site is http://edcimswww.cr.usgs.gov/ pub/imswelcome/.

One way to detect the flooded area is based on the supervised classification of the actual image considering from the differences from a monthly cloud free image derived in the normal season (*Low et al*, 2004). This method is work- and time-consuming. Our aim was to develop an automatic method to create water mask in a faster, easier, and more objective way.

Usually NDVI (Normalized Difference Vegetation Index) and/or the 0.87 μm reflectance are used for water detection, as those have low values at flooded surfaces (and these data have the highest spatial resolution among the MODIS data).

$$NDVI=(R_{0.87}-R_{0.66})/(R_{0.87}+R_{0.66}), \tag{1}$$

where $R_{0.66}$ and $R_{0.87}$ are the reflectance values in channel 2 and 1.

The 0.87 μm reflectance and the NDVI are much lower for water surfaces than for vegetation or bear soil, so this is a good tool for detecting pixels fully covered by clear water. But, unfortunately, for mixed pixels partly covered by vegetation, the NDVI and the 0.87 μm reflectance value can strongly increase, they are sensitive to vegetation portion or turbid water.

Only one test for NDVI is not sufficient, application of more tests is certainly needed if we want to detect not only 100% clear water pixels far from snow, clouds, and cloud shadows. The aim was to find an automatic algorithm to detect pixels that were either 100% water or partially water covered.

At HMS, an automatic cloud detection method for NOAA images was developed (*Kerényi et al.*, 1995). This algorithm has been routinely used at the Hungarian Meteorological Service for years. As an analogue for this cloud detection algorithm, a method for water detection using multispectral MODIS images was developed.

The threshold technique works for each pixel separately. It investigates spectral characteristics of the pixels individually, without taking into account the adjacent pixels. The method consists of more tests, each test examines whether the measured value in a channel (or a value calculated from more channels) is larger (or smaller) than a predefined threshold. If a given combination of the tests fulfils, then the pixel is considered as covered by water.

The main thing is to find the appropriate tests (with physical meaning) and the appropriate thresholds. The thresholds should be general in the meaning that they should not vary from image to image (some seasonal variation may occur, but this should also be predetermined).

For finding general thresholds, the most important thing is to use calibrated (not raw) data. Water detection algorithm works with channels measuring reflected solar radiation, so it is very important to eliminate the effects of illumination conditions. This elimination can be performed by using calibrated values, namely solar zenith angle corrected reflectances. So, the next step was to find the tests, and their accurate combination.

As we have already stated, the NDVI and the 0.87 μm reflectances are useful for clear water detection. The channel 1.6 μm is also very useful for water detection, because it is characterized by the lowest water reflectance and mostly independent of turbidity, which is typical for flood waters. The reflectance in 1.6 μm channel is less affected by vegetation, than the 0.87 μm channel reflectance. Oancea and her colleagues (*Oancea et al.*, 2003) made reflectance measurements at several wavelengths and they confirmed this behavior. The spatial resolution in the 1.6 μm channel is only half as much, as for the 0.87 μm channel, but it is so informative, that we decided to use it for the main test: (i) For water, the 1.6 μm reflectance should be less than a threshold. The problem is that this 1.6 μm channel test can not be used alone. The 1.6 μm channel allows separating water from low-land areas, but not from snow in mountainous areas. Snow is bright in 0.87 μm channel, but dark in 1.6 μm channel. To mask out snowy areas, the 0.87 μm channel was used additionally; (ii) The 0.87 μm reflectance should be less than this threshold. For water both test-conditions should be fulfilled at the same time.

Other problems encountered were caused by orographic and cloud shadows, and by melting snow. Their spectral characteristics were quite similar to those of water, so only partial separation could be achieved. Large, clear water surfaces without vegetation have NDVI values less than –0.2, and

they can be easily separated from shadows. However, using this threshold would mask out not only the shadows but also many pixels containing water, such as the pixels with high vegetation fractions, turbid waters, and mixed pixels along the coasts. To avoid the loss of such pixels, an NDVI threshold greater than –0.2 had to be used.

As a conclusion, three tests were decided to use: first for channel 1.6 μm, a second for channel 0.87 μm and a third for NDVI. For water all the tests should be fulfilled (*Putsay,* 2003). The thresholds can have seasonal variations. Good thresholds must be tested on many images under many circumstances, in different seasons.

We had to make a compromise (*Putsay*, 2004), considering it was not fully possible to separate the water and cloud shadow pixels automatically. In a few cases, cloud shadows were misdetected as water pixels.

The water detection method was developed in two ways:

- The first one is an automatic method, which is quick, but it can misdetect some shadow pixels as water, and it does not detect some water pixels.
- The other method is semi-automatic, which is more accurate, but it needs more time and interactive correction.

3.3.1 The automatic method

The thresholds of the automatic method can be used if there is no time for *a posteriori* manual correction. The following thresholds were derived:

$$(R_{1.6} < 1\%) \text{ or } [(R_{1.6} < 5\%) \text{ and } (R_{0.87} < 13\%) \text{ and } (NDVI < T)], \quad (2)$$

where T varies between –0.2 and +0.2 depending on the seasons and the cloudiness, $R_{1.6}$ and $R_{0.87}$ are the reflectance in channel 1.6 μm and 0.87 μm, respectively. If the 1.6 μm reflectance is very low (less than 1%), then no additional tests are needed.

3.3.2 The semi-automatic method

The semi-automatic method is more accurate, but it needs interactive correction (removal of misdetected cloud shadow vectors manually). For the investigation solar zenith, bow-tie, and geo-corrected MODIS images were used at the time of the flood event in spring 2000 on Körös rivers. A semi-automatic method has been developed by modifying the thresholds and the equation. After the automatic method there is more shadow, but an accurate water mask is got. First, the water mask raster image is derived, then it is

converted to vectors, and third, the misdetected cloud shadow vectors are removed manually.

The new equation and the thresholds are the following:

$$(R_{1.6}<1\%) \text{ or } [(R_{1.6}< 10\%) \text{ and } (R_{0.87}<18\%) \text{ and } (NDVI < 0.4)] \text{ or } [(R_{1.6}< 15\%) \text{ and } (R_{0.87}<15\%) \text{ and } (NDVI < 0.0)]. \quad (3)$$

For a lower *NDVI* value, higher $R_{1.6}$ values are permitted to keep pixels with less water portion.

In *Figs. 2* and *3* water masks derived for three successive flooded days are seen. In *Fig. 1* the lower small white box represents this investigated area. Two-two water vectors are visualized corresponding to different days together to see the variation of the inundated area. In *Fig. 2* water vectors were overlaid on a channel 0.87 μm image as a background (which was taken on April 21), while in *Fig. 3* the vectors were visualized on ASTER land use map.

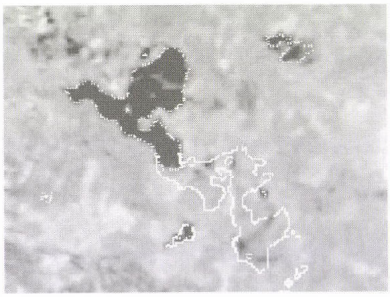

Fig. 2. Water masks derived for two days using MODIS images, visualized on a channel 0.87 μm image (taken on April 21, 2000). The solid line water mask corresponds to the 9th, the dotted line water mask to the 21st of April.

Fig. 3. Water masks derived for two days using MODIS images, visualized on land use map derived from ASTER images. The gray water mask corresponds to April 21, and the black one to May 2, 2000.

4. Validation of water mask

To validate the satellite based water detection method, it was compared with a flood map made by Water Resources Research Center (VITUKI, Hungary) using aerial images. As they had air photos only for Tisza river, the validation was done for the upper Tisza region, for the flood event on Mach 7, 2001. The investigated area is represented by the upper white box in *Fig. 1*. The VITUKI-map is a flood map, it shows only the flooded area, but it does not

contain the river itself, while the MODIS water mask contains the overflowed rivers, as well. *Fig. 4* shows the water-covered area, flooded rivers derived from the MODIS images (black), and flooded area performed from the air photo (light gray). The medium gray patches are the settlements. In *Fig. 4a* the flooded area derived from aerial images are over the water covered area derived from the MODIS images, while in *Fig. 4b* the MODIS water mask is over. As we can see, the MODIS water covered area shows good agreement with the flooded area derived from air photos. Only at the edge of the flooded area we can see difference. The reason of the misdetection is the different spatial resolution between the MODIS and the air photo. At the edge of the flooded area, the MODIS pixels contain water and surface as well, while in the air photo – because of the resolution – they can be separated much better.

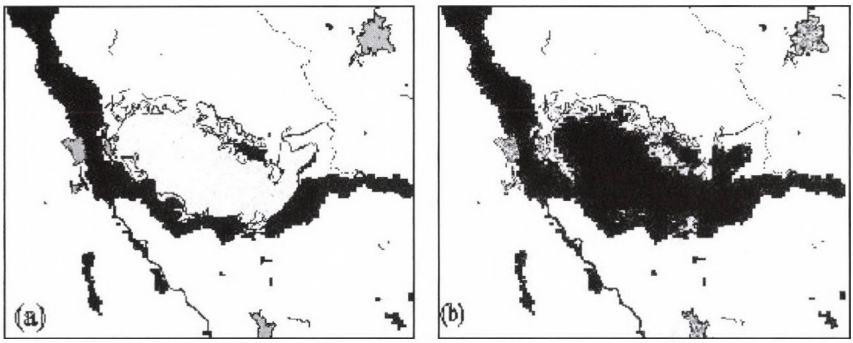

Fig. 4. Water mask (containing flooded area and river) based on MODIS images (black) and flooded area map derived from air photo (light gray) for the Tisza river on March 7, 2001. Medium gray patches are the settlements. The flood map derived from air photos is put over the other on map (*a*) and below on map (*b*).

5. Conclusions

The paper gave a brief overview of the satellite data processing techniques needed for the "Monitoring of Extreme Flood Events in Romania and Hungary Using Earth Observation (EO) Data" in the framework of NATO Science for Peace (SfP) project developed at the Hungarian Meteorological Service (HMS). Our task was to produce a high-resolution land use map about the study area and to develop a method for floodwater detection.

Land use map will be used as background information with topographical, physiographical, and hydrological parameters in the GIS database. It is derived by applying 15 m spatial resolution ASTER images.

Two methods were developed for water detection using multispectral MODIS images. Both methods are based on thresholds techniques. One is automatic, quick, but less accurate, it may contain misdetected cloud shadow pixels. The other algorithm is a semi-automatic method, more accurate, but interactive correction is needed if the investigated area is partly cloudy. The results were compared with air photo. The flooded areas derived from MODIS data and air photo showed good agreement, except at the edge of the flooded, area because of the spatial resolution of MODIS images.

Acknowledgements—This work was supported by the NATO Science for Peace (SfP) Program by the project "Monitoring of Extreme Flood Events in Romania and Hungary Using Earth Observation (EO) Data". We are grateful for the staff of Dartmouth Flood Observatory (Hanover, USA), *G. Robert Brakenridge*, *Emily S. Bryant,* and *Elaine Ande*rson, who helped our work with advices and data. We also thank the staff of VITUKI, *János Szekeres*, *Béla Zóka,* and *Béla Licskó,* who helped at the validation.

References

Guangyu, W., 2005: Seasonal Change Detection of Water Quality in Texas Gulf Coast. Available on-line from http://www.ucgis.org/summer03/studentpapers/guangyuwu.pdf. Accessed March, 2005.

Kameyama, S., Zhang, J., Wang, Q., Xu, K., Katoh, T., and *Watanabe, M.*, 2003: An Approach to Estimate the Water Level and Volume of Dongting Lake by using Terra/MODIS data . *The 2nd APEIS Capacity Building Workshop, November 24-29, Sydney, Australia.* Available on-line from http://www.word-craft.net/nies/english/products/2nd_Sydney/1st-day_2003-11-28/10_ kame.pdf.

Kerényi, J., Szenyán, I.G., Putsay, M., and *Wantuch, F.*, 1995: Cloud detection on a threshold technique for NOAA/AVHRR images for the Carpathian Basin. *Proc. of the 1995 Meteorological Satellite Data Users' Conference*. Winchester, United Kingdom, 4-8 Sept 1995, 565-569.

Low, J., Liew, S.C, and *Kwoh, L.K.*, 2004: Automated Near-realtime Flood Detection and Mapping Using Terra Modis. *Proc. of the 25ht Asian Conference and 1th Asian Space Conference on Remote Sensing*, November 22-26, 2004, Chiang Mai, Thailand. Available on-line from http://www.gisdevelopment.net/aars/acrs/2004/b_change/acrs2004_b2001pf.html.

Oancea, S., Alecu, C., and *Bryant, E.*, 2003: MODIS water classification report. *Report* prepared at the Dartmouth Flood Observatory, 2003.

Pinilla, C., Ariza, F.J., and *Sánchez de la Orden, M.*, 2000: Unsupervised classification's optimization. *Proc. of the 19th EARSeL Symposium on Remote Sensing in the 21st Century*. Valladolid, 31 May–2 June 1999: *Remote Sensing in the 21st Century, Economic and Environmental Applications*, Balkema Rotterdam, 2000, 19-22.

Putsay, M., 2003: Creating a Water Mask using a Threshold Technique on Multispectral MODIS Images. *Report of Visit of Maria Putsay to Dartmouth Flood Observatory*, November 25, 2003. http://nato.inmh.ro/Download/putsay_report.zip.

Putsay, M., 2004: Creating Water Mask using a Threshold Technique on Multispectral MODIS Images. http://nato.inmh.ro/MEDIA/nato2_presentations.html.

Rabaute, Th., Gonzales, Gh., Dupouyet, J.P., Vidal, J.J., Colin, Y., and *Denave, B.*, 2002: Space technologies for flood risk management: from images to products and services. *Proc. of the 21st EARSeL Symposium.* Paris, 14-16 May, 2001: *Observing our environment from Space, New solution for the new milleneum*, Balkema Rotterdam, 2002, 227-235.

Zhan, X., Sohlberg, R.A., Townshend, J.R.G., DiMiceli, C., Carroll, M.L., Eastman, J.C., Hansen, M.C., and *DeFries, R.S.*, 2002: Detection of land cover changes using MODIS 250 m data. *Remote Sens. Environ. 83*, 336-350.

IDŐJÁRÁS

Quarterly Journal of the Hungarian Meteorological Service
Vol. 109, No. 4, October–December 2005, pp. 217–232

Satellite-based analysis of the urban heat island effect

Zsuzsanna Dezső, Judit Bartholy* and **Rita Pongrácz**

Department of Meteorology, Eötvös Loránd University
P.O. Box 32, H-1518 Budapest, Hungary
E-mail: tante@nimbus.elte.hu, bari@ludens.elte.hu, prita@elte.hu

(Manuscript received in final form September 10, 2005)

Abstract—Analysis of the urban heat island (UHI) effects for the Budapest agglomeration area and other nine cities located in Hungary has been accomplished. Remotely sensed information (namely, observations of sensor MODIS on satellites Terra and Aqua) serve as a basic tool to this analysis. Day-time and night-time surface temperature time series have been considered in order to define the UHI intensity as the difference between spatially averaged surface temperature of the urban and surrounding pixels. Spatial structures of the UHI have been determined and compared depending on seasons. The most intense UHIs occur in day-time during the summer months in case of all the selected cities.

Key-words: urban heat island effect, surface temperature, satellite imagery, sensor MODIS, Budapest agglomeration area, Hungarian large cities.

1. Introduction

Increasing human presence and intense anthropogenic activity have a considerable impact on the environment resulting in global change. One of the main aspects includes the increase of artificial covers (e.g., concrete, asphalt) and dense urban areas. Urban conditions significantly modify the surface-atmosphere energy budget and produce the so-called urban heat island (UHI) effect (*Howard*, 1833; *Oke*, 1982). Traditionally, UHI analysis uses air temperature data observed at standard height (1,5–2 m above the ground), while remotely sensed information is often available at ground-level. UHI effect has been investigated using satellite imagery for three decades. The early studies (e.g., *Rao*, 1972) evaluated coarse resolution satellite data (7–8 km per

* Corresponding author

pixel), and used very simple methods to calculate the surface temperature from the spectral observations (*Carlson et al.*, 1977; *Price*, 1979). These investigations in the 1970s and 1980s concluded that satellite measurements can be applied to detect the UHI effect in case of clear sky conditions. The thermal differences between urban and rural areas appear even in case of relatively small towns (*Matson et al.*, 1978; *Price*, 1979). Ground-based measurements require either the installation of a dense station network or the introduction of a measuring equipment mounted on a moving vehicle. Moving measurements can be arranged in a relatively small city, where the difference between observation times may be handled by following the designed path back and forth. In case of several Hungarian cities (e.g., Szeged, Debrecen, Szombathely), *Unger et al.* (2001) and *Bottyán et al.* (2005) accomplished such observations. However, for larger agglomerations, i.e., Budapest, these methods cannot be implemented due to economical constrains. An alternate method using satellite imagery providing spatially continuous and simultaneous observations may be applied to analyze UHI effect of large urban areas as well as smaller cities (*Bartholy et al.*, 2001, 2004; *Rigo* and *Parlow*, 2004). The maximum of the UHI intensity occurs a few hours after sunset using the ground-based air temperature data, while it can be detected during day-time in case of using satellite images (*Roth et al.*, 1989). Nowadays, the main objectives of the UHI investigations include (i) to determine the detailed structure of the UHI (*Nichol*, 1996), (ii) to use this information in the urban planning and human comfort studies (*Scherer et al.*, 1999; *Gómez et al.*, 2001), and (iii) to model wind and temperature patterns of cities (*Herbert et al.*, 1998; *Voogt* and *Grimmond*, 2000). In this paper, the UHI effects for the Budapest agglomeration area and the other nine largest cities of Hungary are analyzed. Besides the capital, the nine most populated Hungarian cities include Debrecen, Miskolc, Szeged, Pécs, Győr, Nyíregyháza, Kecskemét, Székesfehérvár, and Szombathely. First, the satellite data is described and the methodology is presented. Then, results of the analysis are presented separately for the capital and the other nine Hungarian cities.

2. Data and methodology

As part of the Earth Observing System Program of the American National Aeronautics and Space Administration (NASA), satellites Terra and Aqua were launched to polar orbit in December 1999, and May 2002, respectively. Satellite Terra is on a descending orbit (10:30 a.m.), while satellite Aqua is on an ascending orbit (1:30 p.m.), both at 705 km height above the surface. Main goal of remote measurements of these missions is to improve our under-

standing of global dynamics and processes occurring on the land, in the oceans, cryosphere, and lower atmosphere (*NASA*, 1999). These measurements and their use play an important role in the development of validated, global, interactive earth system models being able to predict global climate and environmental change accurately enough to assist policy makers worldwide in making decisions concerning the protection and management of our environment and natural resources. The planned lifetime of satellites is about 15 years. The first observations of satellite Terra started in February 2000, and regular validated measurements are available from July 2000. Numerous climatic and environmental parameters are accessible via Internet at the Earth Observing System Data Gateway.

Five instruments are included in satellite Terra (*NASA*, 1999): (1) ASTER (Advanced Spaceborne Thermal Emission and Reflection Radiometer), (2) CERES (Clouds and the Earth's Radiant Energy System), (3) MISR (Multi-Angle Imaging Spectroradiometer), (4) MODIS (Moderate Resolution Imaging Spectroradiometer), and (5) MOPITT (Measurements of Pollution in the Troposphere). Satellite Aqua carries six instruments: (1) AIRS (Atmospheric Infrared Sounder), (2) AMSU-A (Advanced Microwave Sounding Unit), (3) HSB (Humidity Sounder for Brazil), (4) AMSR-E (Advanced Microwave Scanning Radiometer for EOS), (5) MODIS (Moderate Resolution Imaging Spectroradiometer), and (6) CERES (Clouds and the Earth's Radiant Energy System).

The measurements of sensor MODIS of the above two satellites have been analyzed in this paper. MODIS measures biological and physical processes on the land and ocean using a cross-track scanning multi-spectral radiometer with 36 electromagnetic spectral bands from visible to thermal infrared (*Barnes et al.*, 1998). From the measurements of MODIS the following parameters are determined: surface temperature (both land and ocean), ocean color, global vegetation, cloud characteristics, snow cover, temperature, and moisture profiles. MODIS is capable of viewing the entire globe daily at high resolution, namely 250 m per pixel in the visible and 1 km per pixel in the infrared channels.

In this paper, day-time and night-time surface temperature time series measured in Hungary are analyzed. Surface temperature is strongly related to surface energy budget, especially, to latent and sensible heat flux. Calculation of surface temperature data is based on thermal infrared measurements of MODIS that are quality controlled and calibrated by surface observations (*NASA*, 1999). In order to determine the surface temperature output, seven spectral bands are used: 3660–3840 nm (channel 20), 3929–3989 nm (channel 22), 4020–4080 nm (channel 23), 8400–8700 nm (channel 29), 10780–11280 nm (channel 31), 11770–12270 nm (channel 32), and 13185–13485 nm (channel 33).

Wan and *Snyder* (1999) developed a model to calculate surface temperature from the spectral observations that can be applied in case of clear weather. This so-called Day/Night MODIS LST (Land Surface Temperature) Method enables us to determine surface temperature and emissivity without preliminary knowing of air temperature and water vapor profiles. The problem is underdetermined, when we attempt to solve temperature and surface emissivity in N bands simultaneously, solely from one-time observation (even if the exact atmospheric conditions are known). We have 2N observations using one set during the day and another one during the night. The unknown variables are N bands emissivities, day-time surface temperature, night-time surface temperature, four atmospheric variables: air temperature and water vapor profiles during day and night, and the anisotropic factor. Altogether we have N+7 unknown variables, thus the radiation transfer equations can be solved if $N \geq 7$.

A linear approximation of the radiation transfer equation in the proximities of reference values of surface temperature and band emissivities results in a simplified form (*Strahler et al.,* 1999). Combining 14 equations together (2×7 bands), the solution for surface temperature and band emissivities should be a linear combination of the band brightness temperatures, each of which corresponds to one of the 14 observations. Components of **x** vector (x_i) can be written as follows:

$$x_i = \sum_{j=1}^{14} w_{i,j} \cdot y_j + w_{i,0} , \tag{1}$$

where **x** is a vector of the 14 variables including surface temperature and band emissivities, y_j is the band brightness temperature for observation j, $w_{i,j}$ ($i=1,\ldots,14$ and $j=1,\ldots,14$) and $w_{i,0}$ are the regression coefficients.

In order to separate urban and rural pixels, the MODIS Land Cover Product (LCP) have been used. The LCP values are based on a 1 km gridded database composited from different MODIS products, namely, land/water mask, albedo, spatial texture, directional reflectance, enhanced vegetation index, snow cover, land surface temperature, and terrain elevation information. These data are composited over a one-month time period to produce a globally consistent, multitemporal database on a 1 km grid as input to classification characterization algorithms. The LCP recognizes 17 categories of land cover following the International Geosphere-Biosphere Program scheme (*Belward et al.,* 1999). Land cover classes are produced by processing the 32-day database, using decision tree and artificial neural network classification algorithms to assign land cover classes based on training data (*Strahler et al.,* 1999).

Since the topography significantly affects UHI, hilly regions have to be eliminated. To this process, the GTOPO30 global digital elevation model (DEM) has been used. This global data set was developed by the U.S. Geological Survey's (USGS) Earth Resources Observation System Data Center (*USGS*, 1996). The horizontal grid spacing of this database is 30 arc seconds (approximately 1 km). GTOPO30 is based on data derived from different sources of elevation information, e.g., Digital Terrain Elevation Data, USGS 1-degree DEM's, International Map of the World 1:1,000,000-scale maps, Digital Chart of the World (*Danko*, 1992).

In the present analysis, the ten largest cities of Hungary with more than 80 thousands inhabitants (Budapest, Debrecen, Miskolc, Szeged, Pécs, Győr, Nyíregyháza, Kecskemét, Székesfehérvár, and Szombathely) have been selected according to the population data of the *Hungarian Ministry of Interior* (2000). Pixel representations of the selected urban settlements (including their rural environment) have been determined from the total 1200×1200 pixels containing the Carpathian Basin at the upper half of the satellite image. Since 20% of the country population live in Budapest (which means ten times more inhabitants in the capital than in any other large cities), furthermore, the differences between the spatial extensions of Budapest and other cities are of similar rate, therefore, the agglomeration of the capital is represented by 50×50 pixels (covering 2500 km^2) from the entire satellite image, while other selected cities are represented by only 30×30 pixels (covering 900 km^2). The representative areas have been divided into urban and rural pixels in case of each city. First, the MODIS LCP is applied to separate urban built-up and rural surrounding areas (upper left panel of *Fig. 1*). Urban part of the total area is defined within the 15 km radius circle around the city center in case of Budapest, while 5 km in case of other Hungarian cities. Rural pixels may be found within a 15–25 km or 5–15 km radius ring around the city center in case of Budapest and the other cities, respectively. Furthermore, hilly regions have been eliminated using the global DEM (upper right panel of *Fig. 1*) when calculating the UHI intensity. The finally separated areas are demonstrated in the lower part of *Fig. 1* in case of the Budapest agglomeration area. *Table 1* summarizes the total number of pixels representing the urban and rural areas in case of each city. Cities located in hilly regions are represented by less pixels than expected because of their real spatial extension. On the base of the spatial averages of observed values converted to urban and rural surface temperature, UHI effects have been analyzed for the selected large cities.

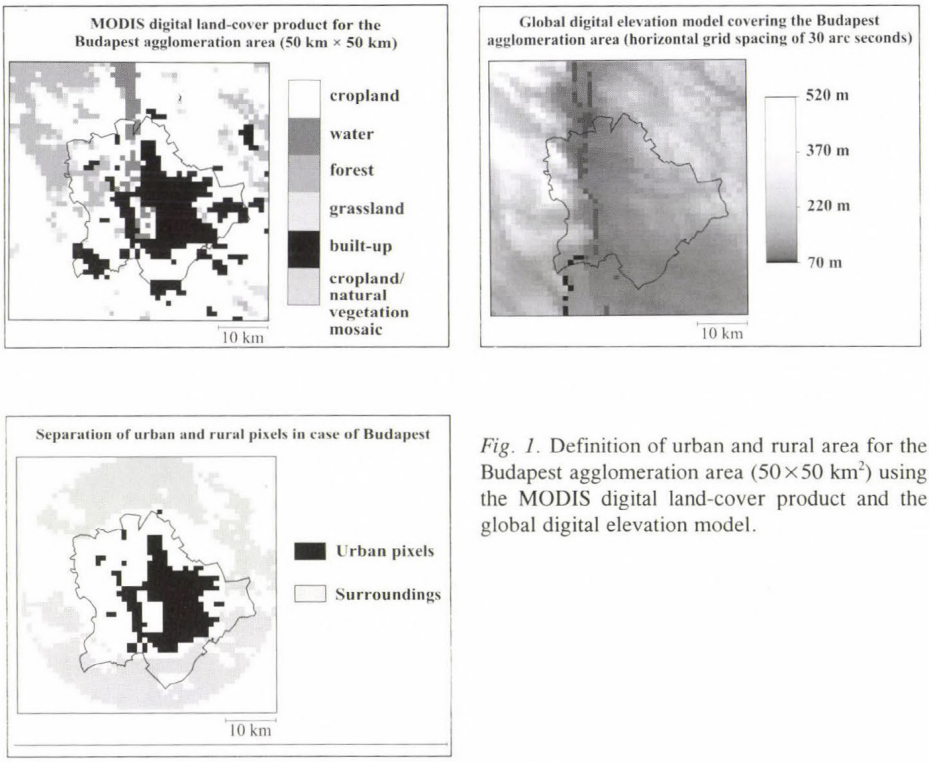

Fig. 1. Definition of urban and rural area for the Budapest agglomeration area (50×50 km^2) using the MODIS digital land-cover product and the global digital elevation model.

Table 1. Number of pixels representing urban and rural area in case of the ten most populated Hungarian cities. The satellite image granule of Budapest contains 2500 pixels, while the granules of the other nine cities contain 900 pixels

City	Urban pixels	Rural pixels
Budapest	237	831
Debrecen	25	621
Miskolc	21	525
Szeged	19	622
Kecskemét	12	624
Nyíregyháza	13	621
Pécs	6	433
Szombathely	10	626
Győr	11	621
Székesfehérvár	7	617

3. *Urban heat island effect of the Budapest agglomeration area*

In this section monthly and seasonal mean spatial structure of the Budapest UHI is presented and compared on the base of the MODIS observations between 2001 and 2004.

Time series of spatial averages of the observed surface temperature in cloud-free urban and rural pixels are determined for each satellite image. Those satellite images, where more than half of the urban pixels were cloud-covered, have been eliminated. In the Carpathian Basin winter days are more often cloudy or foggy than summer days, therefore, less satellite images could be used in winter to calculate the monthly mean UHI intensity, as the difference between the urban and rural average surface temperature, than in summer. *Fig. 2* presents the monthly mean UHI intensity of the Budapest agglomeration area based on remotely sensed surface temperature observed by Terra/MODIS and Aqua/MODIS in 2004. Annual variation of UHI intensity is larger in day-time than in night-time due to larger variance of the energy balance. The most intense UHI effect (4–5 °C on monthly average) occurs during day-time in the summer months in case of both satellites. Direct solar radiation and thermal inertia can be considered as possible reasons.

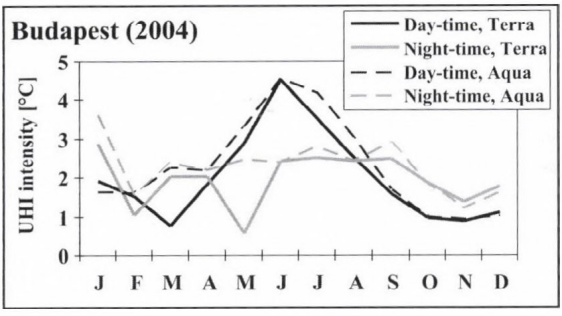

Fig. 2. Monthly mean UHI intensity of the Budapest agglomeration area based on Terra/MODIS and Aqua/MODIS observations, 2004.

The detailed spatial structure is illustrated in *Fig. 3*, where seasonal mean UHIs of day-time and night-time are presented based on Aqua/MODIS thermal information observed in 2004. The seasonal mean difference between the surface temperature of each pixel and the rural mean is presented on the maps. The largest anomaly values and consequently, the most intense UHI occur in summer. UHI intensity is large also in spring, however, smaller anomalies can be detected than in summer.

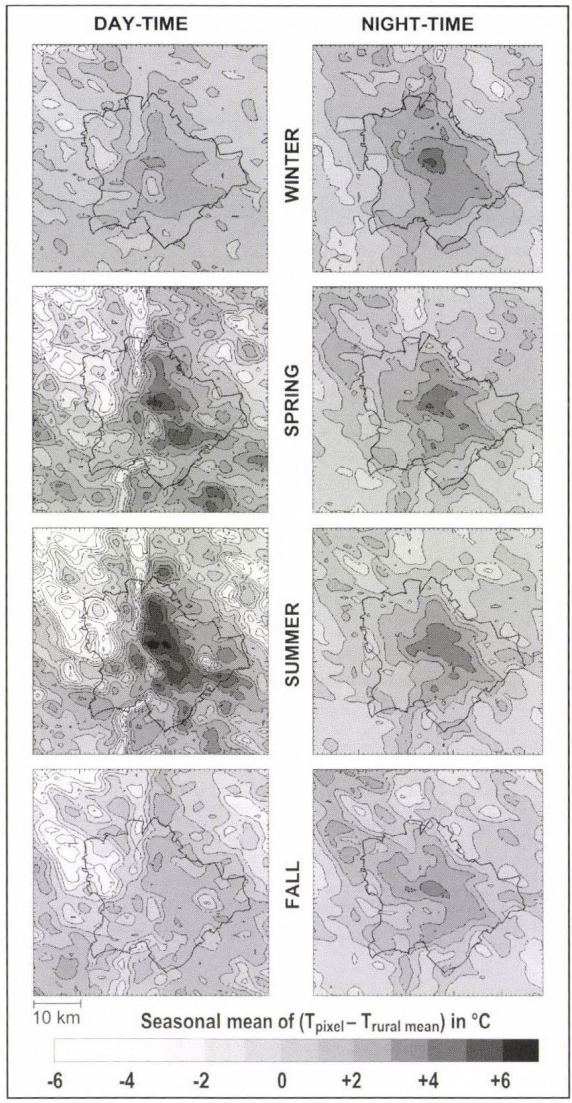

Fig. 3. Annual variation of the seasonal mean UHI structure in Budapest (50×50 km^2) based on Aqua/MODIS observations, 2004.

The maps of *Fig. 3* suggest, that night-time structures of UHI are quite similar to each-other, while UHI structures significantly differ from one another in day-time. The warmest part of the city is the downtown area

(administrative and commercial center) on the left bank of the river Danube (which is on the right side of the presented maps). The western part of the city is hilly and covered by forests, so its surface is relatively cold. The difference between the warmest and coldest surface temperature exceeds 12 °C in summer, and 8 °C in spring. The downtown warm spots are 4–5 °C colder on winter days than on summer days, while the seasonal difference is considerably smaller during nights (less than 1 °C).

In order to analyze the temporal variation of the UHI structure of the Budapest agglomeration area, time series of the monthly mean differences of surface temperature of each pixel and the rural mean along the major cross-sections (i.e., N-S, W-E, NW-SE, NE-SW) have been compared. In this paper, the NW-SE cross-section is selected and shown in *Fig. 4*, because it represents the orographical variability of the capital and its surroundings the most. Since the validated, good-quality measurements are available from 2001, the previous year is not presented here. The four-year-long time series (2001–2004) are calculated from the Terra/MODIS observations. The downtown region can be clearly recognized due to the positive anomaly values that are greater than +5, +6 °C, and +3, +4 °C in day-time and night-time, respectively. Annual variation of the monthly means is more pronounced in day-time than in night-time, which was expected. The maximum anomaly occurs in summer months in both cases. Although record temperature values were detected in Europe in summer 2003 (*Vidale et al.*, 2004), the time series of remotely sensed surface temperature do not show this extreme hot weather. On the contrary, day-time UHI of summer 2003 is weaker than in the other three years analyzed in this paper.

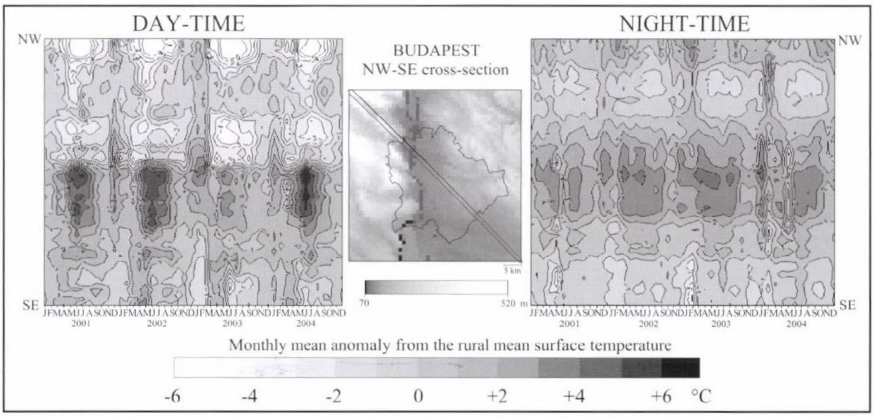

Fig. 4. Monthly mean surface temperature anomaly in the NW-SE cross-section of Budapest agglomeration area based on Terra/MODIS observations, 2001–2004.

Verification of our satellite-based results was accomplished using ground-based observations at the urban climate station installed at the Eötvös Loránd University in 1999 (with the supervision of the Hungarian Meteorological Service). Satellite-based surface temperature and ground-based temperature observations (i.e., 12 UTC, grass minimum, daily minimum, daily maximum, and daily mean temperature values) have been compared (*Bartholy et al.*, 2004). The linear relationship between the satellite- and ground-based temperature measurements were determined, and correlation coefficients of the time series were calculated. Our results suggest very strong relationships with correlation coefficients being larger than 0.91 (in some cases 0.97). Furthermore, other techniques are planned to make verification of the satellite data for larger areas (both in the capital and the other nine cities).

4. Urban heat island effect of the other Hungarian cities

Similarly to the analysis of the Budapest agglomeration area, UHIs of the other nine Hungarian cities are analyzed in this section. *Fig. 5* presents the monthly mean UHI intensity observed in 2004.

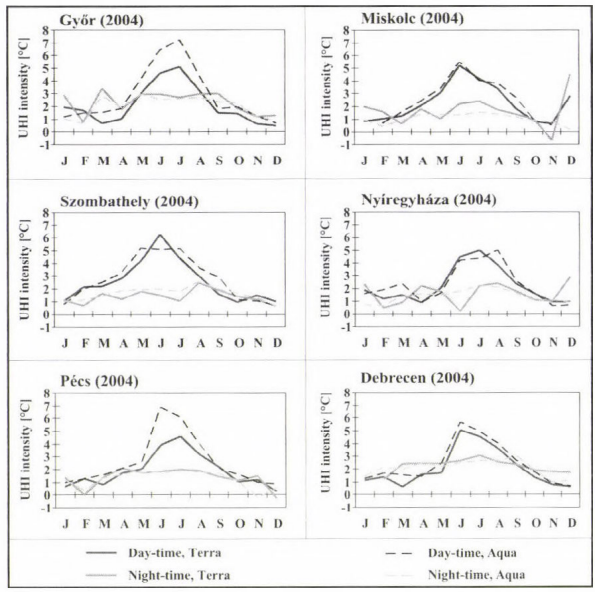

Fig. 5. Monthly mean UHI intensity of selected cities located in Transdanubia (on the left) and Eastern Hungary (on the right).

Graphs on the left side of the figure refer to cities located in Transdanubia, while those on the right side represent the Eastern Hungarian cities. The results suggest that the annual variation of monthly mean UHI intensity is larger in day-time than in night-time, as it was detected in *Fig. 2* in case of the capital, as well. The maximum UHI intensity exceeds 5 °C, and it occurs in day-time from May to August. Usually, day-time monthly mean UHI intensities calculated from the Aqua/MODIS observations are slightly greater than those from Terra/MODIS observations. This can be explained by the orbital parameters of the satellites, namely, the difference between the local times, when the path of the satellites allows to make remotely sensed measurements of the Carpathian Basin. Satellite Terra crosses our region earlier (around 8–11 o'clock) than satellite Aqua (around 10–13 o'clock). Therefore, thermal radiation values observed by satellite Terra are slightly less than those of satellite Aqua.

Temporal evolution of UHIs can be analyzed using different cross-sections of the surrounding region of the cities. Day-time and night-time monthly mean surface temperature anomalies relative to the monthly rural means are determined for each pixel in the 30×30 km^2 surrounding of the nine Hungarian cities. *Figs. 6* and *7* summarize the time series of pixels located in the N-S or W-E cross-sections of the selected regions for the Transdanubian and Eastern Hungarian cities, respectively. The presented cross-sections have been selected on the base of the representativeness of the geographical and orographical features in case of each city. According to the results, the most intense UHIs occur in summer day-time as in case of the Budapest agglomeration area. Another similarity between Budapest and the other nine cities can be recognized, namely, the day-time variation is greater than the difference between the monthly means during night-time. However, due to the evident difference between city sizes, spatial extension of UHI is smaller in case of these nine cities than in case of the capital. On the base of *Figs. 6* and *7*, besides the UHI effect, seasonal variation of other land cover types (e.g., river, forest) and orographical features (e.g., valleys, hills) can be evaluated. For instance, in case of the N-S cross-section of the satellite image subsection containing Győr (on the top of *Fig. 6*), the river Danube can be well identified due to the large seasonal variation of surface temperature anomalies in day-time. In the summer half-year, large negative values can be detected in these pixels. Other examples can be seen in case of Pécs and Miskolc (bottom of *Fig. 6* and top of *Fig. 7*, respectively), where hilly regions and valleys are located in the presented cross-sections. As an opposite of the positive anomaly values of the UHI, the hilly (mountain Mecsek) or the valley (valley of the creek Szinva in mountain Bükk) negative anomalies appear with large seasonal variation in day-time. The difference between the warm UHI and the cold hilly or valley region is the greatest in the summer months.

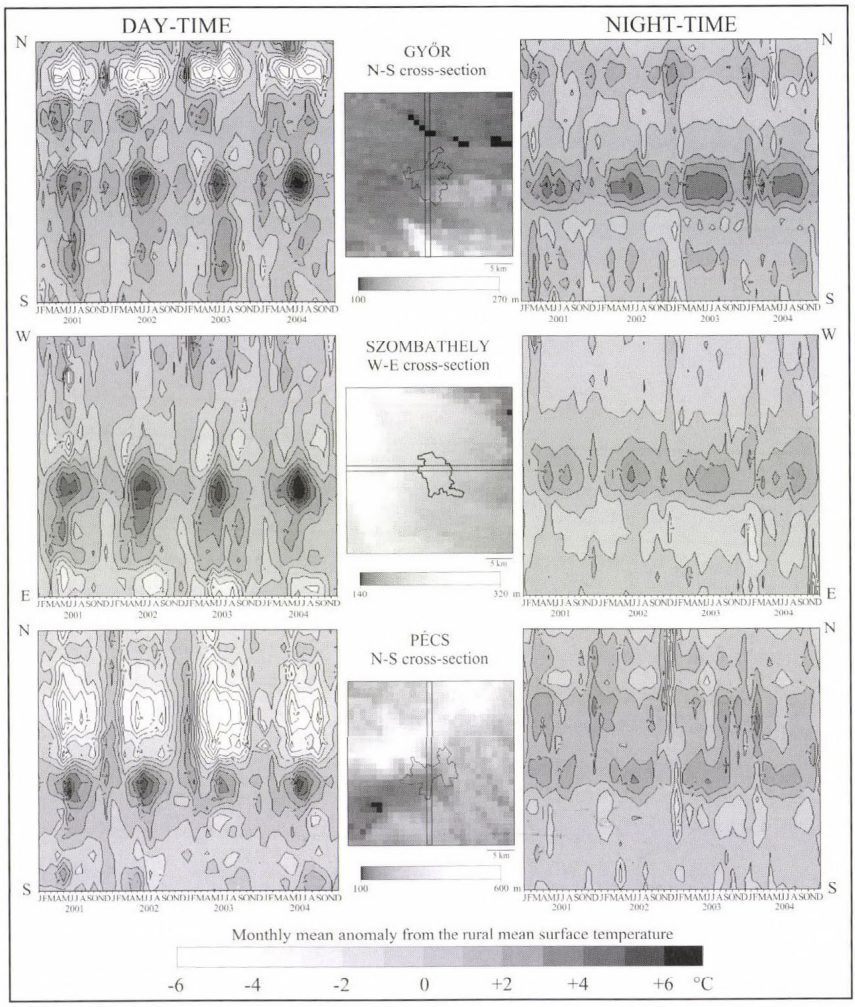

Fig. 6. Time series of monthly mean surface temperature anomaly in case of selected Transdanubian cities in the characteristical cross-sections based on Terra/MODIS observations, 2001–2004.

Mean UHI intensity is shown in *Fig. 8*, where the cities are ranked according to the number of their inhabitants starting with the capital. The UHI intensity presented here is calculated using the Terra/MODIS night-time observations between 2001 and 2004. Basically, more populated cities exhibit more intense heat island, and only orographical modification disturbs this relationship by decreasing the UHI intensity. Since Budapest, Miskolc, and

Pécs are located in hilly regions, partly or entirely, their mean UHI is less intense than expected. Although the city of Kecskemét is small, its central location on the Great Plains may explain the larger mean difference between the temperature of urban and rural areas. Finally, in case of Győr, the surroundings contain several cold spots because of the large floodplain of the river Danube that results in more intense UHI than expected.

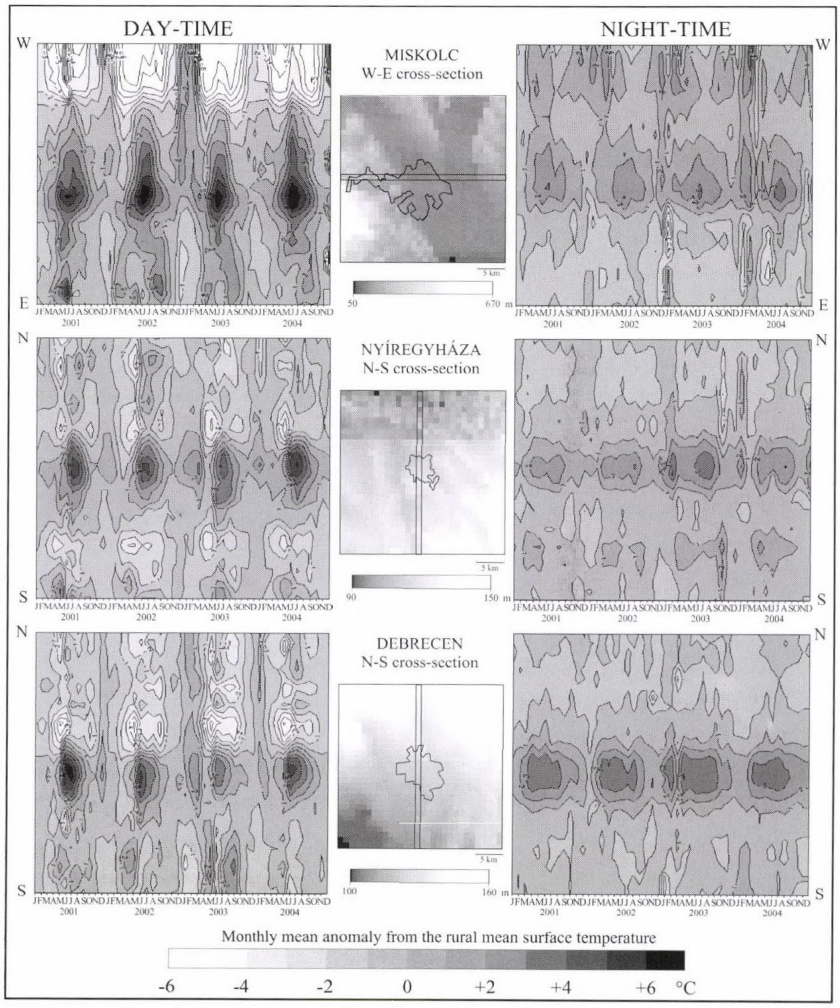

Fig. 7. Time series of monthly mean surface temperature anomaly in case of selected Eastern Hungarian cities in the characteristical cross-sections based on Terra/MODIS observations, 2001–2004.

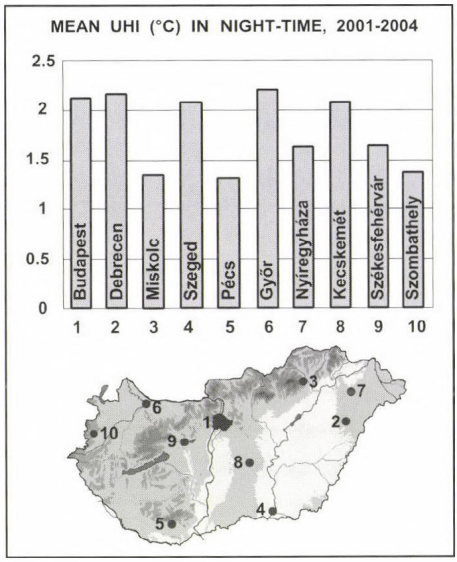

Fig. 8. Mean night-time UHI intensity of the ten most populated cities of Hungary, 2001–2004.

5. Conclusions

In order to find potential mitigation strategies that facilitate the urban population to adapt to new environmental conditions, UHI and other climatological impacts of urbanization should be investigated. In this paper, the ten most populated cities of Hungary (including the capital) have been selected, and their urban and rural pixel representations have been determined. Day-time and night-time surface temperature time series measured by the instrument MODIS of satellites Terra and Aqua have been analyzed. Urban and rural spatial averages have been calculated and compared for each selected city. Monthly and seasonal mean spatial structures of UHI have been determined. On the base of the results the following conclusions can be drawn:

- No significant difference can be detected between the UHI intensity values based on the MODIS-observations of the two satellites (Terra and Aqua).
- Day-time UHIs exhibit greater monthly variation than night-time UHIs in case of both the Budapest agglomeration area and the other nine Hungarian cities. The maximum UHI effect can be detected in day-time.

- The most intense UHI occurs in the summer period (May-June-July-August) for all the urban sites. Monthly mean UHI intensity in these months exceeds 5 °C.
- In the Budapest agglomeration area, the difference between the warmest and coldest surface temperature exceeds 12 °C in summer, and 8 °C in spring. The downtown warm spots are 4–5 °C colder on winter days than on summer days. The seasonal difference is much smaller during night-time.

Acknowledgements—The authors wish to thank NASA for producing the satellite surface temperature data in their present form and the Earth Observing System Data Gateway for distributing the data. Research leading to this paper has been supported by the *Hungarian National Science Research Foundation* under grants T-034867, T-038423, and T-049824, also by the AEROCARB and CHIOTTO projects of the *European Union* Nr. 5 program under grants EVK2-CT-1999/0013, EVK2-CT-2002/0163, and the *Hungarian National Research Development Program* under grants NKFP-3A/0006/2002 and NKFP-3A/082/2004.

References

Barnes, W.L., Pagano, T.S., and *Salamonson, V.V.*, 1998: Prelaunch characteristics of the Moderate Resolution Imaging Spectroradiometer (MODIS) on EOS-AM1. *IEEE T. Geosci. Remote 36*, 1088-1100.

Bartholy, J., Pongrácz, R., and *Dezső, Zs.*, 2001: Evaluation of urban heat island effect for large Hungarian cities using high resolution satellite imagery. *Proc. of the Fifth European Conference on Applications of Meteorology, ECAM 2001* (ed.: *M. Hunkár*). Kiadó? Budapest.

Bartholy, J., Pongrácz, R., Barcza, Z., and *Dezső, Zs.*, 2004: Aspects of urban/rural population migration in the Carpathian Basin using satellite imagery. In *Environmental Change and its Implications for Population Migration* (eds.: *J.D. Unruh, M.S. Krol,* and *N. Kliot*) Book series "*Advances in Global Change Research*" Vol. 20. Kluwer Academic Publishers, Dordrecht and Boston, 289-313.

Belward, A.S., Estes, J.E., and *Kline, K.D.*, 1999: The IGBP-DIS 1-Km Land-Cover Data Set DISCover: A Project Overview. *Photogramm. Eng. Rem. 65*, 1013-1020.

Bottyán, Zs., Kircsi, A., Szegedi, S., and *Unger, J.*, 2005: The relationship between built-up areas and the spatial development of the mean naximum urban heat island in Debrecen, Hungary. *Int. J. Climatol. 25*, 405-418.

Carlson, T.N., Augustine, J.A., and *Boland, F.E.*, 1977: Potential application of satellite temperature measurements in the analysis of land use over urban areas. *B. Am. Meteorol. Soc. 58*, 1301-1303.

Danko, D.M., 1992: The digital chart of the world. *GeoInfo Systems 2*, 29-36.

Gómez, F., Tamarit, N., and *Jabaloyes, J.*, 2001: Green zones, bioclimatic studies and human comfort in the future development of urban planning. *Landscape Urban Plan. 55*, 151-161.

Herbert, J.M., Johnson, G.T., and *Arnfield, A.J.*, 1998: Modelling the thermal climate in city canyons. *Environ. Modell. Softw. 13*, 267-277.

Howard, L., 1833: *Climate of London Deduced from Meteorological Observations*. Vol. 1-3. Harvey and Darton, London.

Hungarian Ministry of Interior, 2000: *Local Authorities Database*. http://web.bm.hu/proba/-cimtar.nsf/lakossag.

Matson, M., McClain, E.P., McGinnis D.F., and *Pritchard, J.A.*, 1978: Satellite detection of urban heat island. *Mon. Weather Rev. 106*, 1725-1734.

NASA, 1999: *Science Writers' Guide to Terra.* NASA Earth Observing System Project Science Office, Greenbelt, MD.

Nichol, J.E., 1996: High-resolution surface temperature patterns related to urban morphology in a tropical city: a satellite-based study. *J. Appl. Meteorol. 35*, 135-146.

Oke, T.R., 1982: The energetic basis of the urban heat island. *Q. J. Roy. Meteor. Soc. 108*, 1-24.

Price, J.C., 1979: Assessment of the heat island effect through the use of satellite data. *Mon. Weather Rev. 107*, 1554-1557.

Rao, P.K., 1972: Remote sensing of urban heat islands from an environmental satellite. *B. Am. Meteorol. Soc. 53*, 647-648.

Rigo, G. and *Parlow, E.*, 2004: Multitemporal analysis of the urban surface temperature – Heat island of the city of Basel. In *New Strategies for European Remote Sensing* (ed.: *M. Oluic*) Milpress, Rotterdam, 679-683.

Roth, M., Oke, T.R., and *Emery, W.J.*, 1989: Satellite-derived urban heat island from three coastal cities and the utilization of such data in urban climatology. *Int. J. Remote Sens. 10*, 1699-1720.

Scherer, D., Fehrenbach, U., Beha, H.-D., and *Parlow, E.*, 1999: Improved concepts and methods in analysis and evaluation of the urban climate for optimizing urban planning processes. *Atmos. Environ. 33*, 4185-4193.

Strahler, A., Muchoney, D., Borak, J., Friedl, M., Gopal, S., Lambin, E., and *Moody, A.*, 1999: *MODIS Land Cover Product Algorihm Theoretical Basis Document, Version 5.0.* Center for Remote Sensing, Department of Geography, Boston University. Boston, MA.

Unger, J., Sümeghy, Z., and *Zoboki, J.*, 2001: Temperature cross-section features in an urban area. *Atmos. Res. 58*, 117-127.

USGS, 1996: GTOPO30 documentation. http://edcdaac.usgs.gov/gtopo30/.

Vidale, P.L., Lüthi, D., Frei, C., Häberli, C., Liniger, M.A., and *Appenzeller, C.*, 2004: The role of increasing temperature variability in European summer heatwaves. *Nature 427*, 332-336.

Voogt, J.A., Grimmond, C.S.B., 2000: Modeling surface sensible heat flux using surface radiative temperatures in a simple urban area. *J. Appl. Meteorol. 39*, 1679-1699.

Wan, Z. and *Snyder, W.*, 1999: *MODIS Land-surface Temperature Algorithm Theoretical Basis Document.* Institute for Computational Earth Systems Science, Univ. of California, Santa Barbara.

IDŐJÁRÁS

Quarterly Journal of the Hungarian Meteorological Service
Vol. 109, No. 4, October–December 2005, pp. 233–256

An evaluation of the performance of the three-dimensional variational data assimilation scheme for the ALADIN/HU spectral limited area model

Steluţa Vasiliu[1] and **András Horányi**[2]

[1]*National Meteorological Administration of Romania*
97, Sos. Bucuresti-Ploiesti, 013686 Bucharest, Romania
E-mail: steluta.vasiliu@meteo.inmh.ro

[2]*Hungarian Meteorological Service*
P.O. Box 38, H-1525 Budapest, Hungary; E-mail: horanyi.a@met.hu

(Manuscript received in final form November 10, 2005)

Abstract—In this paper, the three-dimensional variational (3D-Var) data assimilation scheme for the ALADIN/Hungary model is described and its performance is evaluated by comparing the resulting forecast scores with those from the reference model running in dynamical adaptation. Experiments with different assimilation strategies have been studied, in order to establish the general framework for further research. The verification scores show a better short-range performance of the 3D-Var system. More results are presented for two individual synoptic cases, corresponding to interesting meteorological situations. One was selected based on the poor performance of the reference model, where the model using the 3D-Var scheme is found to perform better. The other was an example, when the operational model did well, and it was shown that the 3D-Var scheme is able to keep the good performance of the reference model.

Key-words: variational data assimilation, 3D-Var, mesoscale limited area model

1. Introduction

Numerical weather prediction (NWP) is a modern discipline in meteorology, which makes the prediction of future states of the atmosphere numerically feasible. In order to produce an accurate weather forecast, a realistic description of the initial atmospheric conditions is required. This is achieved basically by using observational information from the atmosphere together with

its assimilation into the numerical model. High quantity of observations is available with large temporal and spatial resolution about the atmosphere from a variety of observing types. Anyway, in spite of the relatively high volume of the observations, they are still considered to be sparse and heterogeneous having in mind the number of all state variables at all model grid points. In other words, the assimilation problem is highly under-determined. Therefore, beside the observations, one must use additional past and current information to improve the initial conditions. The most important such information is the *background* or *first guess*, which is nothing else, than a short range forecast of a numerical weather prediction model valid at the analysis time (i.e., the time instant, when the initial conditions for the NWP model are to be determined).

The ultimate goal of the atmospheric data assimilation is to produce a regular, dynamically consistent four-dimensional representation of the atmospheric states from observations irregularly distributed in space and time, taking into account first guess information and considering all the error characteristics of the applied information sources. This latter is needed for the evaluation of the reliability of the information source in the assimilation process. Since all information has to be represented within the NWP model, it is important, that the model has a sufficiently high resolution, with physically realistic detail.

In 1987, ECMWF together with Météo-France established the basis of a new forecasting system. The main goals of this project were to develop efficient global data assimilation tools (4D-Var system), and also to have numerical weather prediction models at every spatial and time scales (*Courtier et al.*, 1991). Thus, the project is named IFS (**I**ntegrated **F**orecasting **S**ystem) at ECWMF, and ARPEGE (**A**ction de **R**echerche **P**etite **E**chelle **G**rande **E**chelle) at Météo-France. In the literature, it is often referred as "ARPEGE/IFS". The models are global spectral primitive-equation models, with a triangular spectral truncation in the horizontal, and a hybrid coordinate in the vertical.

In 1990, Météo-France started a collaboration with several weather services, mainly from Central and Eastern Europe, in order to develop a limited area version of the ARPEGE/IFS model, in the framework of the existing global code, for dynamical adaptation at the limit of the hydrostatic approximation. The new model, called ALADIN (**A**ire **L**imitee **A**daptation dynamique **D**eveloppement **I**nter**N**ational), is a spectral mesoscale limited area model (LAM), using bi-Fourier horizontal spectral representation. An important part of the ARPEGE dynamics is kept and its physics is basically identical with the ARPEGE's one (*Horányi et al.*, 1996; *Pailleux*, 1997).

A data assimilation system had been under development since 1996 for the ALADIN LAM, based on a three-dimensional variational (3D-Var) scheme. Being counterpart of the global model ARPEGE, the ALADIN 3D-Var system

basically follows the specifications of the ARPEGE version. ALADIN has specific code only in the horizontal part (because of the geometry), but in the vertical part, the observation operators and vertical grids are identical for both models. The main goal of the ALADIN 3D-Var system with the analyses of such high density observations, which are not assimilated by the ARPEGE assimilation system, is to analyze better the small scales of the atmosphere, without touching the large scales already analyzed in the global model.

Our work was devoted to the development and application of the ALADIN 3D-Var scheme to the ALADIN/HU version of the model applied at the Hungarian Meteorological Service. Thus, the first experiments of the 3D-Var data assimilation scheme for the ALADIN/HU model were aiming to get a general impression of the applicability of the scheme and, moreover, to establish the best possible strategy for such a mesoscale data assimilation system. Many experiments were performed in this framework in order to choose, beside others, the lateral boundary conditions to provide the large scale information, the first guess to be used, the optimal initialization method to be applied, the way to incorporate the lateral boundary conditions, etc. These experiments provided the framework for a more detailed study of the application of the 3D-Var scheme. The next set of experiments was performed by choosing special meteorological situations, where on the one hand, the reference version (without data assimilation) failed to provide a good prediction, and on the other hand, where the operational (reference) forecast was reasonably good. For the first synoptic case the improvements were checked, and in the latter one, whether the new scheme is able to keep the good performance of the model.

The present paper describes the latest results obtained using the 3D-Var scheme for a spectral mesoscale limited area model. A brief overview of the formulation of the 3D-Var scheme in the ALADIN model is given in Section 2. Section 3 presents the experiments, which helped to establish an optimal assimilation strategy. Afterwards, the results of two case studies are illustrated in Section 4. The conclusions are summarized at the end, and finally some plans for the future are presented briefly.

2. Data assimilation method for the ALADIN model

The limited area model ALADIN is running in dynamical adaptation mode in many European countries. This means that no independent objective analysis is performed in order to obtain initial conditions for the limited area model, instead the large scale forecasts, provided by the global model ARPEGE, are adapted to the high-resolution local characteristics (whence the name

"dynamical adaptation"). The lateral boundary coupling is carried out using the Davies relaxation technique (*Davies*, 1976), where the relaxation zone of the domain ensures the continuous transition between the boundary conditions and the ALADIN solution obtained every time-step.

Another algorithm to be used for the ALADIN model is the 3D-Var data assimilation scheme for providing initial conditions of the model. The code for the 3D-Var scheme for the ALADIN model is basically the same as for the ARPEGE global model, with some differences because of the applied geometries (spherical for the global model, and plane Cartesian grid for the limited area model). Thus, the horizontal interpolations from the model grid to the observation position, and also some required physical transformations, are performed in a different way. This split presents the advantage that allows introducing the geometrical specificities to the horizontal operators (especially the ALADIN domain aspects), while retaining all the ARPEGE code in the vertical part, since the vertical grids and observational operators are identical for ARPEGE and ALADIN.

The 3D-Var cost function for the ALADIN/HU model is a sum of the background term and observation term. No constraint term was introduced so far in the ALADIN/HU 3D-Var system. The observation term might take into account different types of observations: conventional (SYNOP, AMDAR/aircraft data, radiosondes, PILOT balloons) and remote sensed (for instance satellite winds, ATOVS radiances) ones. For the background term, the standard NMC statistics are considered. The NMC (National Meteorological Center, now is called National Centers for Environmental Prediction) method estimates the background error statistics using a set of differences between forecasts valid at the same time, but at different ranges (usually 36h–12h differences) (*Parrish* and *Derber*, 1992). Statistical balance is considered between the model variables (vorticity ξ, divergence η, temperature T, logarithm of surface pressure P_s, and specific humidity q), where the empirical balance coefficients are obtained from multiple regressions over the set of those NMC differences, and provide a set of uncorrelated variables used as predictors in the analysis, instead of the model variables. This method was used first for the global model (ARPEGE), and then it was adapted for the high-resolution limited area model with an additional balance relation for humidity. Thus, for the ALADIN model, the relationships between predictors and predictands are as follows:

$$\begin{aligned}
\xi &= \xi, \\
\eta &= \mathbf{MH}\xi + \eta_u, \\
(T, P_s) &= \mathbf{NH}\xi + \mathrm{P}\eta_u + (T, P_s)_u, \\
q &= \mathbf{QH}\xi + \mathbf{R}\eta_u + \mathbf{S}(T, P_s)_u + q_u,
\end{aligned}$$

where ξ, η, (T, P_s), and q are the forecast errors of vorticity, divergence, temperature and surface pressure, and specific humidity, on models levels. The subscript u stands for unbalanced (total minus balanced) fields. **M**, **N**, **P**, **Q**, **R**, and **S** are the vertical balance operators. They are block-diagonal matrices relating spectral vertical profiles of predictors and those of the predictands. **H** is the horizontal geostrophic balance operator. It transforms vorticity ξ into the so-called balanced geopotential $P_b = \mathbf{H}\xi$ (*Berre*, 2000).

The 3D-Var system of the ALADIN/HU model particularly performs four analysis steps each day, with observation window of six hours, centred on the observing times at 00, 06, 12, and 18 UTC. Each analysis step begins with the observation pre-processing, when a quality control for the observation format and position, for the climatological and hydrostatic limits, and for the temporal consistency is realized. Another criterion to check the observation is to compute and compare the innovation vector of each observation to its expected values defined by the diagonal of the observational error covariance matrix. In this way the best-quality and unique observations close to the analysis time are selected.

Further, the 3D-Var analysis is performed, using the background information, the observation file prepared by the screening (quality control) and the background error statistics. The ALADIN/HU 3D-Var system is using a quasi-incremental procedure, only that the analysis increment and the first guess have the same resolution. The pre-conditioning is used for a faster convergence of the minimization of the cost function. So first the differences between the background field and the observations are calculated. The analysis increments are estimated using the observation increments. Afterwards, these increments are used to update the background field in order to create the analysis. The minimization is based on a variable-storage quasi-Newton algorithm (*Gilbert* and *Lemaréchal*, 1989). Because the 3D-Var data assimilation scheme is acting only for the upper-air meteorological fields, after the variational analysis step, the optimal interpolation method is applied for the surface variables. In principle, this step can be performed prior to the upper-air variational analysis step as well. Each analysis is used to initialize the forecast model, which is integrated for a six-hour range (at least for the assimilation runs). However, for production mostly 24-hour and 48-hour forecasts are carried out. The six-hour forecast is used as first guess of the following analysis. The refreshment of the lateral boundary conditions is done every 6 hours in our case. During these experiments the horizontal resolution of the ALADIN/HU model is 8 km.

The experiments described below have been performed with the 3D-Var data assimilation scheme for the *double-nested limited area model*, ALADIN/HU. Double nesting means that the boundary conditions of the

model are provided by another limited area model, ALADIN/LACE (**L**imited **A**rea modelling for **C**entral **E**urope), which has a larger domain, and a lower resolution. At its turn, this limited area model is driven by the global model ARPEGE. The idea of the double-nested models is to get a fine scale resolution in the area of interest, and to analyze better the physical processes from the smaller scales with a reasonable computational cost.

3. General evaluation

A general evaluation of the ALADIN/HU 3D-Var system was realized, before any other detailed studies were performed, especially because there were so many choices in order to establish the optimal strategy for the 3D-Var scheme.

In the assimilation process, both the information from the first guess and from the observations are important for the quality of an analysis. For the global models (in intermittent data assimilation cycles), the first guess is always the 6-hour forecast from the previous model integration. But for the mesoscale models, different possibilities can be chosen: the 6-hour forecast from the previous model integration (the classical choice), which contains information from the small scales, the analysis provided by the global model, which contains information mainly from the large scales, or the mixture of the first two information, with the help of some kind of *blending* procedure, which merges the fine-mesh information from the limited area model, and the synoptic scale information from the analysis of the global model. For the time being, the 6-hour forecast from the previous integration of the model as first guess for ALADIN/HU 3D-Var system has been considered a natural choice. A blending between the ALADIN/HU forecast, using the 3D-Var data assimilation scheme, and the ARPEGE analysis is considered in a later stage.

3.1 Coupling strategies

Another question was the way in which the information from the lateral boundary conditions (LBC) should be incorporated into the data assimilation cycle. Two different strategies were tested. The first one is the so-called "time-consistency" coupling technique, when the lateral boundary conditions, necessary for the integration of the limited area model, contain time consistent tendency information, being provided by the same integration of the coupling model. The second strategy, named "space-consistency", differs from the previous one, that the 3D-Var analysis replaces the first lateral boundary condition, thus the information for the integration of the model is consistent in space. In practice it means that the initial field and the first LBC field are the

same. The first experiments were performed for a period of one week, when the two coupling techniques have been systematically compared in terms of verification scores.

For the experiments, the background error statistics are determined by the standard NMC method, and the observation term takes into account surface and upper-air (radiosounding) observations. Thus, the relative humidity, geopotential, and temperature measurements are assimilated from the surface data, and geopotential, wind, temperature, and relative humidity variables from the radiosondes.

All the data assimilation experiments were run with a six-hour cycle (the integration length of the background field), and 24 hours in production (for the short-range forecast of the model). Digital filter initialization (DFI) has been applied both in cycling and production. Analyses and forecasts were verified against radiosondes, using mainly simple statistical measures, as mean error (BIAS) and root mean square error (RMSE). These objective scores are calculated for the results of the model using 3D-Var scheme, and also of the operational one (in dynamical adaptation), with respect to the observations. The compared fields are the temperature, geopotential, zonal and meridional wind, relative humidity, direction and speed of the wind. Also other objective measures, as time-evolution of the fields at different levels of the model, have been examined. For subjective evaluation, maps with analysis increments and representation of different meteorological fields were drawn.

During the evaluation of the verification scores, we have to keep in mind, that the 6-hour forecast (from 00 UTC and 12 UTC model runs) is compared with the data from 06 UTC and 18 UTC, respectively. For these moments of time, the number of observations is much smaller than at 00 UTC and 12 UTC. This means that the statistical scores for 06 UTC, as an example, do not have the same precision, as those for 00 UTC. But even in this situation, the scores give a general idea about how the forecast using the 3D-Var data assimilation scheme is behaving compared to the operational one.

The vertical cross section of RMSE scores for relative humidity and geopotential are plotted in *Fig. 1*, for the analysis of the operational model, and of the model using 3D-Var scheme, in time-consistency and space-consistency. The most significant improvements, meaning better scores of the analyses, have been obtained for the relative humidity (*Fig. 1*, left panel) and wind (not shown). There is a slight advantage for the 3D-Var scheme for temperature (not shown) and geopotential (*Fig. 1*, right panel) for some upper levels, otherwise the scores are almost neutral. Comparing the curves, when the two different coupling techniques have been applied, it reveals that the model using the 3D-Var scheme with the time-consistency coupling technique has slightly better scores.

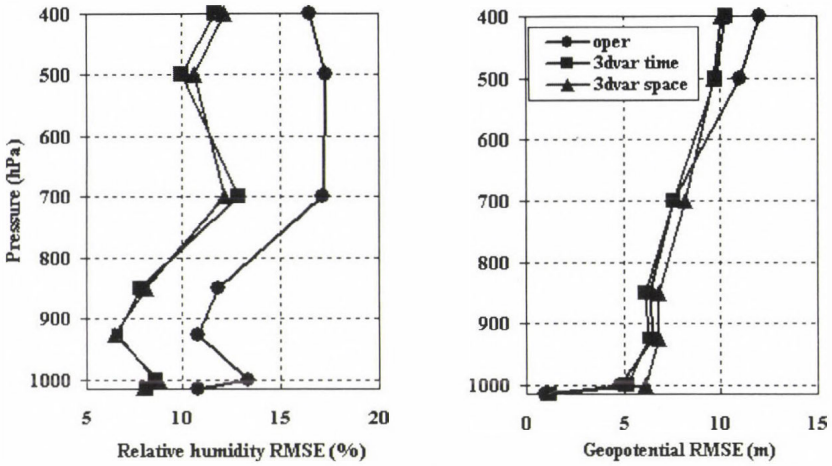

Fig. 1. Vertical profile of the RMSE of the operational analysis (*oper* – line with circles) and using 3D-Var scheme in time-consistency (*3dvar time* – line with squares), and space-consistency (*3dvar space* – line with triangles), for relative humidity (left panel) and geopotential (right panel).

Verifications of the 6-hour forecasts illustrate, that when the 3D-Var scheme has been used, the forecasts lost from the initial improvements, especially for wind and relative humidity (*Fig. 2*, left panel). But still the model using the 3D-Var scheme was able to provide a better forecast for relative humidity especially up to the middle troposphere. For the other upper levels, the operational model has been slightly improved the six-hour forecast. Verification of geopotential (*Fig. 2*, right panel) and wind generally showed a more positive impact of the 3D-Var scheme, than those of temperature, for which the scores were neutral. Wind forecasts are sometimes better for some upper levels using the 3D-Var scheme than in dynamical adaptation, and sometimes it is the reverse. Regarding the two coupling techniques, the verification scores for the six-hour forecast show again that the results of the 3D-Var system using the time-consistency technique were improved mainly for the relative humidity and wind fields.

After 24-hour integration, the scores are very similar to those in dynamical adaptation, with small variations near the surface (not shown). This means that the information is coming mainly from the lateral boundary conditions, as for the operational forecast, and the impact of the observational data assimilated at the beginning of the forecast period becomes negligible.

In conclusion, the scores showed that the 3D-Var analysis fits the observations for all the fields reasonably well, as it was expected of a data

assimilation scheme. The 6-hour forecast of the model using 3D-Var scheme is losing from the initial improvement, but not for all levels. After 24-hour integration, the scores start to be very close to each other. These verification scores and also other objective measures helped us to choose "time-consistency" as coupling technique for the experiments using the 3D-Var scheme for the ALADIN/HU model.

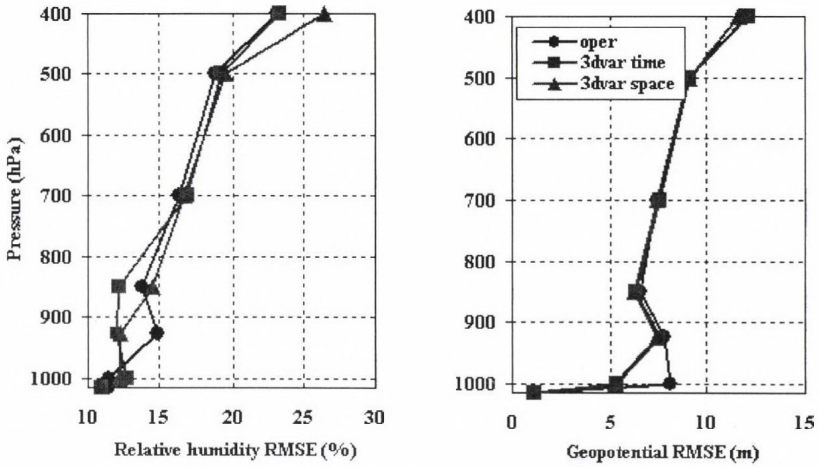

Fig. 2. Vertical profile of the RMSE of the operational 6-hour forecast (*oper* – line with circles) and using 3D-Var scheme in time-consistency (*3dvar time* – line with squares), and space-consistency (*3dvar space* – line with triangles), for relative humidity (left panel) and geopotential (right panel).

3.2 Initialization methods

Further we tried to decide which initialization method is better for application both in cycling and production. As it was mentioned before, the ALADIN model is using the digital filter initialization (DFI) technique, to suppress the unrealistic high-frequency gravity oscillations from the initial conditions. A variation of the classical DFI method has been tested, namely the incremental digital filter initialization (IDFI), when it is assumed that the first guess is already balanced and the analysis increment (the difference between the analysis and the first guess) should be filtered. The third choice was not to apply any initialization method in the 6-hour assimilation cycle. The same time period was selected as for the previous experiments.

Similarly to the previous experiments, first the verification scores have been examined, and they show a neutral impact of the different initialization

methods. Thus, it was difficult to select which method is better to be applied. So, further other objective measures were used, like the time evolution of some fields at different levels, in order to check the balance properties of the different fields. *Fig. 3* shows the time evolution of mean sea-level pressure checked during the 6-hour integration in cycling for a selected case (February 28, 2002, 00 UTC), for four different points on the domain. The selected points were chosen accordingly: two are over the mountains, one is in the middle of the domain, and the other one is in the left-bottom corner of the domain.

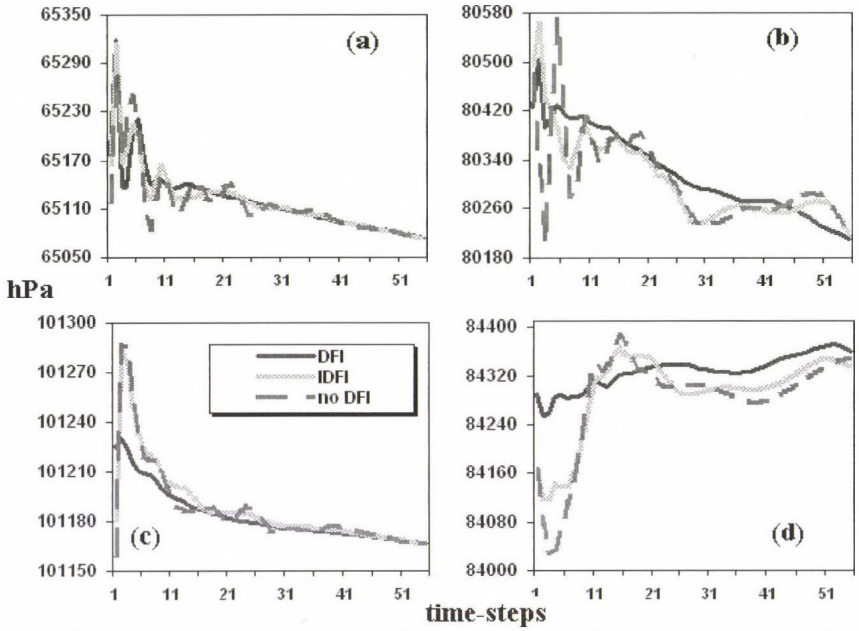

Fig. 3. Time evolution of the mean sea-level pressure using different initialization methods in cycling, DFI (solid line), IDFI (dotted line), no DFI (dotted-dashed line), for February 28, 2002, 00 UTC. (*a*) and (*b*) represent points in mountainous regions, (*c*) a corner point, and (*d*) a point in the middle of the domain.

The noise can be seen for the first time-steps of the integration, when no initialization or IDFI were used in the assimilation cycle. The curves when DFI was applied are rather smooth. At the end of the six-hour forecast, the level of noise looks relatively small, even without DFI or IDFI. But one can

see, that for some points, six hours are sometimes not enough to get a filtered forecast. So we could consider, that the final 6-hour forecast has bigger chance to be realistic if it results from a less noisy time evolution. In conclusion, the digital filter initialization has been selected to be applied in cycling.

The time evolution of the mean sea-level pressure was checked during the 6-hour integration in production (not shown), for the operational forecast and using 3D-Var scheme with different initialization methods in cycling and production. It seems that the fields are in balance, when DFI was used in production (for the operational model, and also with 3D-Var scheme). Without initialization, the noise appeared especially for the first time-steps. Following the same argument as before, it was decided that digital filter initialization has to be applied also in production (*Alexandru*, 2002).

3.3 Lateral boundary conditions

Another experiment was carried out using different lateral boundary conditions provided by the driving model (ALADIN/LACE) and global model (ARPEGE) in the assimilation cycle. The time period of these experiments was extended to one month.

The verification scores of analyses, provided by the operational model and using the 3D-Var scheme with different lateral boundary conditions, against observations are presented for temperature and zonal wind. The temperature scores show an advantage for the 3D-Var scheme for all the upper levels (*Fig. 4*, left panel). Comparing with the first experiments (for the one week period), one can say that the significant improvement in the analyses of wind is illustrated again (*Fig. 4*, right panel). Geopotential scores are almost neutral for the lower levels for both models (with and without data assimilation), but above 700 hPa, the 3D-Var scheme has a slight advantage (not shown). Another field estimated well by the model with the data assimilation was the relative humidity (not shown). Generally, the model using the 3D-Var scheme was able to provide a better analysis. Anyway, the main interest during these experiments was to see whether or not the choice of the lateral boundary conditions (from the ALADIN/LACE or ARPEGE models) is important. No large difference could be seen for the analysis verification, for all the fields (*Alexandru*, 2003).

The six-hour forecast scores for temperature (*Fig. 5*, left panel) show that the models, using the 3D-Var scheme and in dynamical adaptation perform equally well, with very small differences near the surface. In terms of the wind, the scores look slightly better using data assimilation than the reference, at almost every upper level (*Fig. 5*, right panel). The verification for relative humidity shows an improvement using the 3D-Var scheme especially near the

surface, whereas for the upper levels, the operational forecast is slightly better (not shown). Compared to the analysis, the forecast of the geopotential, with data assimilation, was improved especially in the lower levels (also not shown). The only difference between the results of the verification of the model using the 3D-Var scheme with different LBCs appeared in the upper levels for the zonal wind, where the LBCs from the ALADIN/LACE model seems to provide a slight improvement.

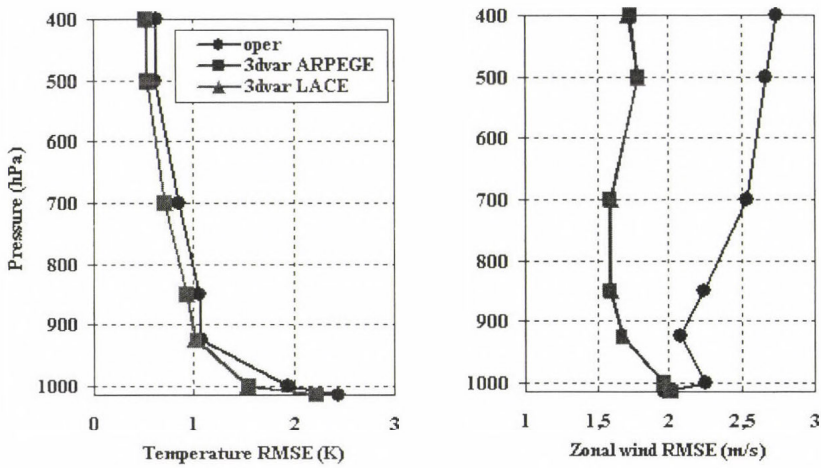

Fig. 4. Vertical profile of the RMSE of the operational analysis (*oper* – line with circles) and using 3D-Var scheme with ARPEGE (*3dvar ARPEGE* – line with squares), and LACE LBCs (*3dvar LACE* – line with triangles), for temperature (left panel) and zonal wind (right panel).

Other objective measures showed small differences on results, when the lateral boundary conditions from the two coupling models were used in the assimilation cycle. Also maps with the representation of some meteorological fields were checked, but again the differences for the experiments with 3D-Var scheme and different LBCs were not visible (not shown).

So far, the general evaluation of the 3D-Var scheme permitted us to conclude, that the optimal choices are as follows: lateral boundary conditions to come from the same integration of the coupling model, thus the information to be consistent in time, and digital filter initialization to be applied both in cycling and production, in order to have a filtered forecast. The choice of the lateral boundary conditions from the global or limited area model is indifferent.

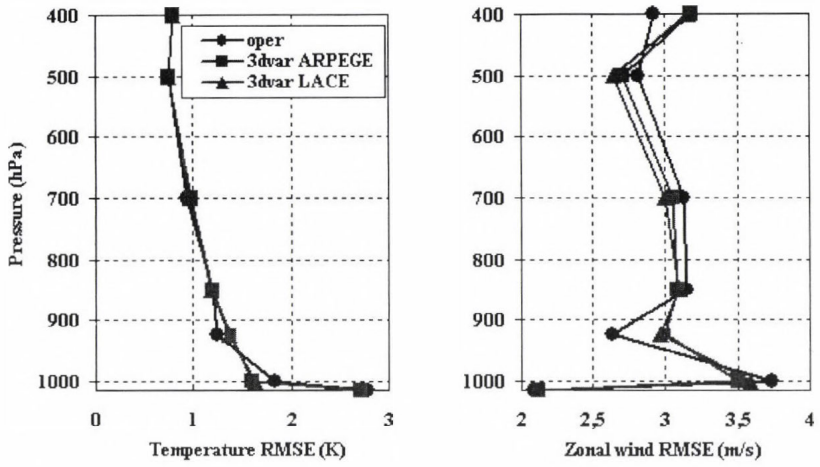

Fig. 5. Vertical profile of the RMSE of the operational 6-hour forecast (*oper* – line with circles) and using 3D-Var scheme with ARPEGE (*3dvar ARPEGE* – line with squares), and LACE LBC (*3dvar LACE* – line with triangles), for temperature (left panel) and zonal wind (right panel).

4. Case studies

Once the best possible scientific strategy of the ALADIN/HU 3D-Var system was established, some interesting meteorological situations have been selected in order to study the performance of the model using the 3D-Var scheme in more details. Thus, two types of cases are presented in this paper: one, when the operational model failed to provide a reasonable forecast, and the second one, when the operational forecast was very accurate. The lateral boundary conditions were provided by the ALADIN/LACE model, using time-consistency as coupling technique, and digital filter initialization was applied in cycling and production (see the previous chapter).

4.1 Summer case (July 17–18, 2002)

A short description of the synoptic situation of this case is as follows. On July 13, a cold trough spread over Western Europe on the 500 hPa isobaric surface. From this, a cold drop isolated on July 14, moved to east, whirled over Northern Italy on July 16, at noon, and filled slightly in between. From noon of July 17, it got a cold supply on the backside, which made the cyclone to strengthen again and to move to east from July 18. Between July 18 and 20, the cyclone moved over the Carpathian Basin. Thus on July 18, large amount of precipitation (up to 54 mm/24h) was measured over the central part of

Hungary, along the Danube river (*Fig. 6*). In the morning of July 18, a steady convergence evolved in the wind field that probably played an important role as a trigger effect in the rainstorm (with precipitation over a large area).

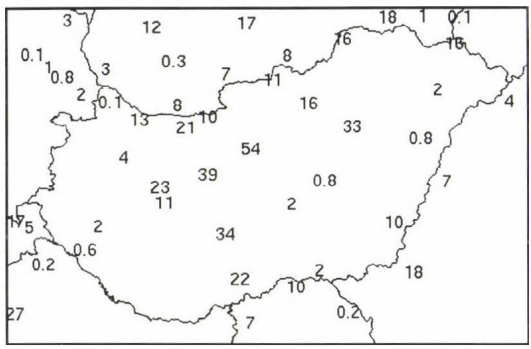

Fig. 6. The amount of precipitation (mm/24h) measured over Hungary between July 18, 06 UTC and July 19, 06 UTC.

For this case study, the results of the ALADIN/HU model, running in dynamical adaptation (the operational version) and using the 3D-Var scheme, were examined. The first one was kept as the reference for all the new experiments with data assimilation. The plots of different meteorological fields (except for the geopotential height forecasts) were zoomed over Hungary, in order to focus on the place of interest.

In *Fig.* 7, the geopotential height forecasts show that the cold air is streaming from north-west in the lower troposphere, bringing cooler air especially in the western part of Hungary. The operational forecast of relative humidity at 700 hPa indicates the availability of moisture in the south-western part of Hungary, and that the area of the Danubian Basin is partly cloudy (not shown). However, the vertical velocity field does not indicate any significant rising motion of the air masses through the 700 hPa surface (also not shown). So, heavy rainfall is not likely to occur in the central part of Hungary. The maximum of precipitation predicted by the model running in dynamical adaptation is located in the south-western part of the country, with a value around 36 mm/24h (*Fig. 8,* left panel). The location of this precipitation maximum is related to the area, where the moisture is available. Compared to real measurements, it can be seen that the operational model misforecasted this event, because no precipitation has been indicated over the Danubian Basin, and the maximum in the south-western part of Hungary was not more than 5 mm/24h.

Comparing the geopotential forecasts of the models with and without data assimilation, one can see the considerable differences, which appeared over Hungary (*Fig. 7*). The assimilation of observations helped the model, using the 3D-Var scheme, to predict a low-pressure system located over the Danubian Basin. The cyclone is well defined also in the altitude.

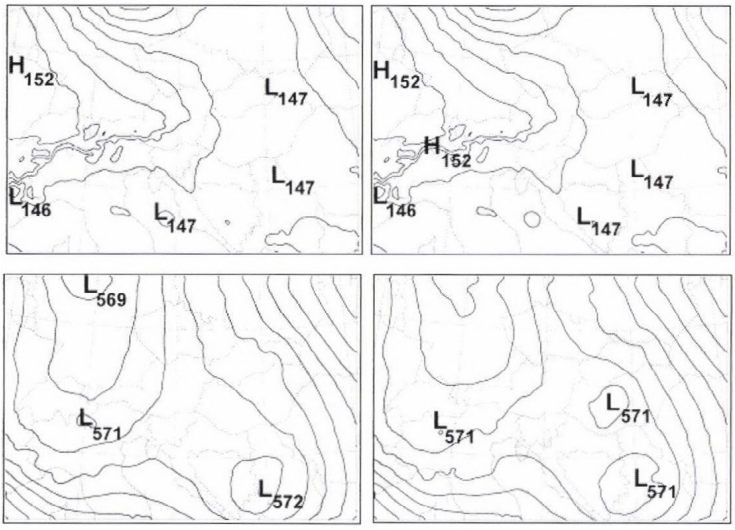

Fig. 7. 18-hour forecasts of the model in dynamical adaptation (left column) and using 3D-Var scheme (right column) for geopotential height (dam) at 850 hPa (upper row) and 500 hPa (lower row), valid on July 18, 18 UTC. For geopotential height the contour intervals are at every 1 dam.

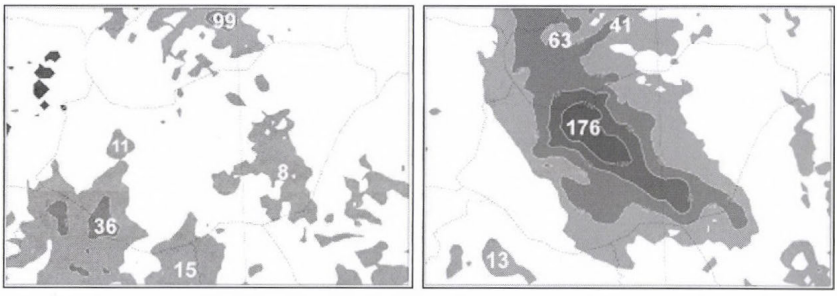

Fig. 8. The amount of precipitation (mm/24h) forecasted by the models in dynamical adaptation (left panel) and using 3D-Var scheme (right panel) over Hungary, between July 18, 06 UTC and July 19, 06 UTC. The contour values are 5, 20, 50, 100 mm/24h.

The area, where enough moisture is available, covers almost the entire country in the experiments when 3D-Var scheme has been used, with a high likelihood of precipitation in the central part, as it is illustrated in *Fig. 9*. Also, the forecast of the vertical velocity field at 700 hPa shows an intensive vertical motion. All these fields, together with the forecast of the low geopotential height gave an indication of the heavy rainfall to be occurred over the central part of Hungary.

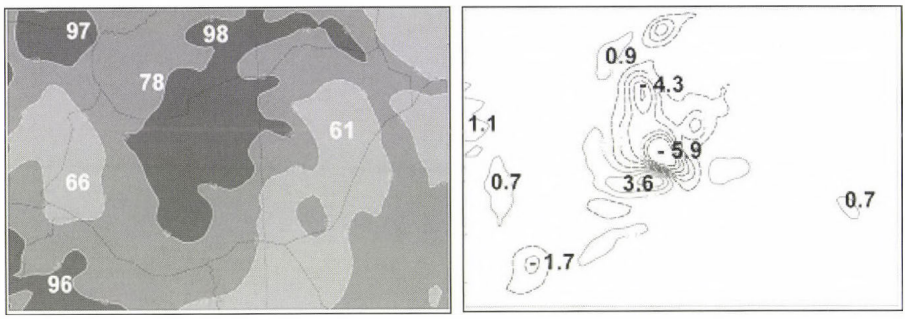

Fig. 9. 18-hour forecasts of the model using 3D-Var scheme, for relative humidity (left panel) and vertical velocity (right panel), at 700 hPa, valid on July 18, 18 UTC. For relative humidity, the contour values are 40, 60, 75, 90%, and for vertical velocity, the contour intervals are at every 0.9 Pa/s.

In *Fig. 10*, the divergence at different upper levels from the experiments with data assimilation is plotted. One can see the strong divergence at 300 hPa and the convergence at 850 hPa, located in the central part of Hungary. In this area the vertical velocity at 700 hPa is around –6 Pa/s, and also the moisture is available. Usually, strong divergence at upper levels, associated with large areas of rising air in the middle troposphere, indicates heavy rainfall.

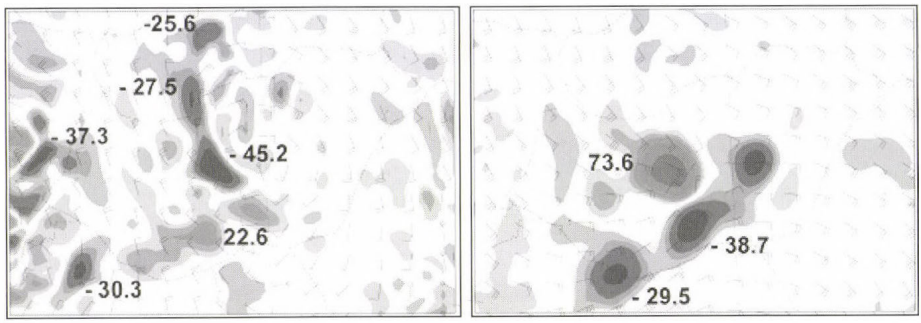

Fig. 10. 18-hour forecasts of wind (m/s) and divergence ($*10^5$/s) at 850 hPa (left panel) and 300 hPa (right panel), valid on July 18, 18 UTC.

The precipitation forecast of the 3D-Var experiments has a good location generally (*Fig. 8*, right panel), being predicted over the entire Danubian Basin, but the amount of rainfall (with the maximum around 176 mm/24h) is much greater than in reality (compared with values as 54 mm/24h). *Fig. 8* illustrates what a big difference was between the precipitation forecast of the two models. So, the assimilation of observations helped the ALADIN/HU 3D-Var system to realize a better prediction of this event, however, the amount of precipitation was overestimated.

Trying to understand how the observations have influenced the quantity and location of precipitation, some experiments were carried out using the 3D-Var scheme, and assimilating only the surface or upper-air (radiosounding) measurements available at the Hungarian Meteorological Service, all along the cycle. The results of these experiments showed, that such set of observations, which are uniquely responsible for the improved prediction of the rainfall event, cannot be identified. The most important features for the forecast are coming from the upper-air observations. However, for this case it is better to use observations from surface and upper-air together. Naturally, the positive influence of the observations over the forecast is bigger as the time is closer to the moment of the event, and as the location of the high resolution data is closer to the area of interest.

As a conclusion from this case study, it can be said that the operational model was unable to predict any features of the phenomenon. Neither the coupling model gave any indication about the rainfall to the coupled model through the lateral boundary conditions. However, the ALADIN/HU model, using 3D-Var scheme, forecasted large amount of precipitation (even too much) as it was in the reality. Therefore, the new information coming from the observations contributed to the improvement of the forecast of this event, in spite of the fact, that some of the applied observations for the limited area model was already used in the global ARPEGE analysis (4D-Var).

4.2 The Czech floods in August 2002

Another case study has been selected in order to be studied using the ALADIN 3D-Var scheme. The operational forecast of this event was considered a success by the forecasters. So the aim of the new experiments was to check whether or not the model using data assimilation can achieve similar performance as it is for the reference version.

In August 2002, disastrous floods hit Central-Europe. The floods proceeded in two waves and were caused by intensive rain from two deep cyclones and the related frontal systems, one following the other at a very short time interval. Both moved slowly, but only the second one was

remarkably well developed. On August 6, a high altitude low-pressure system from the Gulf of Genoa reached the area of the Alps causing rain showers and thunderstorms in Austria. As an effect of the moist air with unstable stratification in the cyclone, the amount of precipitation was high, 50–100 mm in the Alps, but in some places of the central part of Austria it exceeded even 200 mm during the two days.

Precipitation in the Alps begun to diminish temporarily between August 8 and 10. Rain showers, thunderstorms continued to occur, but significant quantity of precipitation fell only locally. A new active cyclone reached Northern Italy on August 11. Because an anticyclone was located over Eastern Europe, first the depression moved slowly in the northeast direction, and then more to the north. Thus, its occluded front spread over the central part of Austria and Bohemia for three days almost without any movement. As a consequence of this stationary front, the quantity of precipitation was again significant in Austria, Bavaria, and Bohemia, reaching 100–150 mm in 24-hour, and locally 200 or in some places even more than 300 mm (*Fig. 11*) (*Sopko*, 2003).

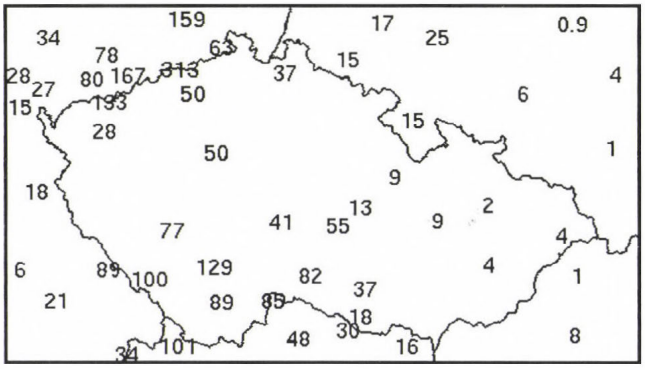

Fig. 11. The amount of precipitation (mm/24h) measured over the Czech Republic between August 12, 06 UTC and August 13, 06 UTC.

Both models, with and without data assimilation, succeeded to predict the slow motion of the cyclone, together with the heavy rainfall. On August 11, the cyclone moved from Northern Italy over Austria, progressing on a northward track. The area where enough moisture was available is very large, covering the western part of Austria, Bavaria, Saxony, and the western part of the Czech Republic. The air masses at that location have an intensive vertical motion (of around -6.5 Pa/s). So there is an increased likelihood that heavy precipitation will develop. Both models predicted almost the same pattern of

high humidity. The location of the rainfall and the very high quantity of precipitation (not shown) were well forecasted. Locally in Austria, the rainfall was overestimated (more than 200 mm/24h), comparing with measurements (100 mm/24h). Also, in the borderline areas of South Bohemia and Austria, the models predicted heavy rainfall.

On the following day, the centre of the low-pressure system moved towards the northern part of Bohemia. The depression has deepened in between, and the rainfall intensified. On the fronts the temperature forecasts showed sharp contrasts, and the air was very warm in the warm sector.

The operational and 3D-Var forecasts of the relative humidity at the 700 hPa isobaric surface showed the same shape of the areas, where the moisture is available (*Fig. 12*). One can see that the air was very humid, especially in the northern part of Austria, Bohemia, and Saxony, with a strong ascending vertical motion. These facts indicate that a heavy rainfall is likely to occur. In the southern part of Austria, the sky is partly cloudy and the air has descending motion (not shown), which are generally associated with areas of fair weather. So it is expected that the precipitation will end soon.

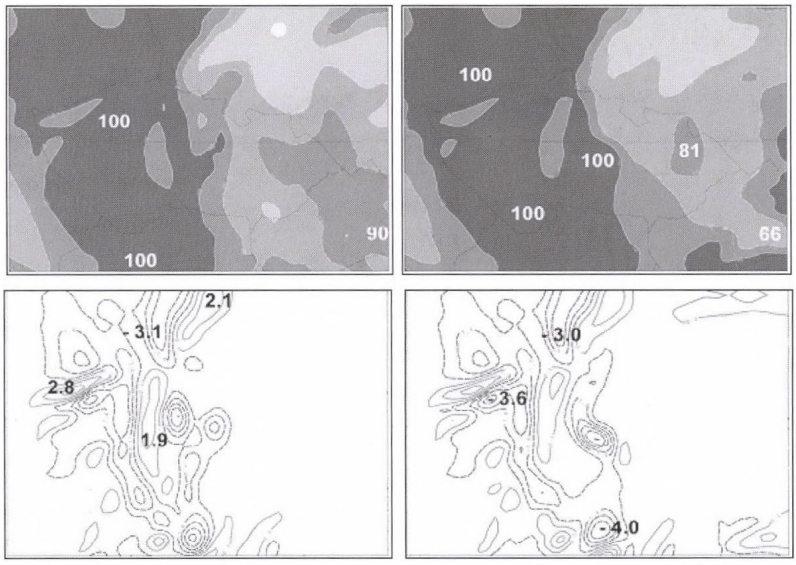

Fig. 12. 24-hour forecasts of the model in dynamical adaptation (left column) and using 3D-Var scheme (right column), for relative humidity (upper row) and vertical velocity (lower row) at 700 hPa, valid on August 13, 00 UTC. For relative humidity, the contour values are 40, 60, 75, 90%, and for vertical velocity, the contour intervals are at every 0.9 Pa/s.

Fig. 13 shows the precipitation accumulated in 24 hours between August 12, 06 UTC and August 13, 06 UTC. Both models predicted the right location of the rainfall in Saxony, where values up to 296 mm/24h are shown. The operational forecast had the closest value to reality. But also the 3D-Var experiments predicted an important quantity in that area. A good prediction of the rainfall over Bohemia has been performed also. A small area with 100 mm precipitation forecast in 24 hours, can be seen over the border of Poland and the Czech Republic. The quantity is overestimated, in reality it has not been more than 37 mm/24h, but it is an indication of the new place, where significant rainfall is expected.

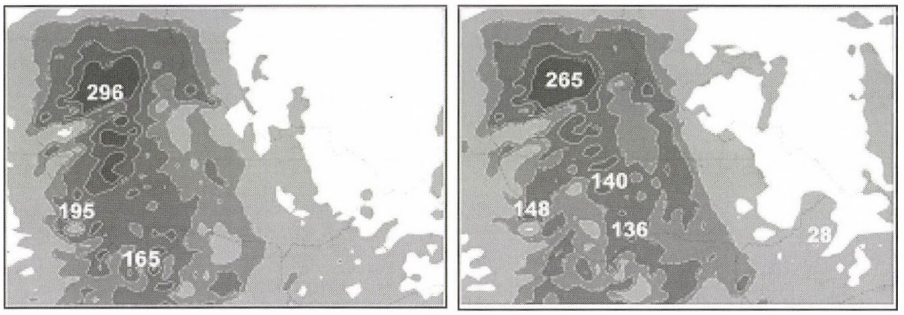

Fig. 13. The quantity of precipitation (mm/24h) forecasted by the models in dynamical adaptation (left panel) and using 3D-Var scheme (right panel) over the Czech Republic, between August 12, 06 UTC and August 13, 06 UTC. The contour values are 5, 25, 50, 100, 150 mm/24h.

On August 13, the forecasts of the models showed that the cyclone continued to move to a north-eastward direction, over Poland. The pressure gradients weakened and the winds subsided, so the cyclone began to fill. The differences between the operational forecasts for geopotential and those of the model using 3D-Var scheme are very small, less than 1 dam. The moisture was available in the south-western part of Poland, the Czech Republic, and the western part of Hungary. The vertical motion of the air masses is less intense, reaching values of 2.6 Pa/s (not shown).

The intensity of precipitation started to decrease, and the location of the rainfall moved towards the eastern part of the Czech Republic. Both models predicted almost the same quantity of rain (cumulated in 24 hours, between August 13, 06 UTC and August 14, 06 UTC), and the location was also similar. Comparing to reality, the models in dynamical adaptation and using the 3D-var scheme showed an underestimation of the amount of precipitation

in some places and an overestimation in others. However, the locations of the maximum values over the border of the Czech Republic and Poland, and in Moravia were well predicted. So the forecast still can be considered good with reasonable limits.

The successful forecast of the operational ALADIN/HU model is partly due to the correct information provided through the initial and more particularly through the lateral boundary conditions. Being a double-nested limited area model, it means that both ALADIN/LACE and mainly ARPEGE models provided a good forecast for the floods. The global model ARPEGE, using 4D-Var scheme, assimilates more types of observations, compared with the 3D-Var scheme for ALADIN/HU model. This is one explanation of the good performance of the global model.

The accurate information from the lateral boundary conditions, together with the assimilation of more surface observations, helped the model with 3D-Var scheme to obtain a good prediction of the event. It was concluded, that the 3D-Var system does not deteriorate the good performance of the reference model.

In this chapter, the results of two versions of the limited area model, with and without data assimilation, in different meteorological situations have been described. It was shown first, that the model using 3D-Var scheme was able to improve the forecast, when the operational model failed. Then, that the 3D-Var scheme can support the model to achieve the same good results, as the operational one succeeded.

5. Discussion and conclusions

In the present paper, the 3D-Var scheme for the double-nested limited area model, ALADIN/HU, has been described, and its performance has been compared to that of the operational version of the model, running in dynamical adaptation. Nevertheless, it is believed that the double-nesting aspect is not really important, while interpreting the obtained results. The experiments were realized in two parts. First, a general evaluation was carried out, in order to establish the best possible framework of the ALADIN/HU 3D-Var system. Then, some synoptic cases have been investigated, in order to study the scheme in greater detail.

For the general evaluation, different sets of experiments with the models in dynamical adaptation and using the 3D-Var scheme have been performed. The statistical scores for the analysis have shown large improvements for relative humidity and wind fields. Also, a positive impact for the temperature and geopotential has been achieved. These scores illustrate that the 3D-Var

analysis fits well to the observations, as it was expected of a data assimilation scheme. In the short range, geopotential and wind fields have been found to be slightly better with respect to the reference throughout the troposphere. Relative humidity kept its improvement also, as it is shown by the forecast scores. But the difference between the two models, in terms of the statistical scores, starts to decrease with respect to time. One explanation can be the deficiency of the verification procedure, due to the fact that the six-hour forecast is compared against a smaller number of the observations than the analysis. As the forecast range increases, the scores of both models are getting closer, which means that the information is provided mainly from the lateral boundary conditions, while the analysis has less influence on the forecast. Regarding the coupling strategy, it has been decided that using all the lateral boundary conditions from the coupling model (i.e., "time-consistency" technique), the fields show a better representation.

The impact of different initialization methods over the analysis and the short-range forecast has been found to be rather neutral in terms of the verification scores, computed with respect to observations. The time evolution of the mean sea-level pressure field during the first six-hour integration of the model using the 3D-Var scheme with different initializations revealed, that in order to obtain a balanced first guess, the digital filter initialization should be applied in cycling. Also, in production it was decided to use the initialization based on the digital filters, to reduce the inertia-gravity waves from the initial conditions.

The statistical scores from the experiments, when the lateral boundary conditions have been provided by different models (global or limited area model), illustrate the positive impact for almost every field when the 3D-Var scheme has been used, compared to the results of the reference model (running in dynamical adaptation). The objective and subjective evaluations revealed similar results between the experiments with the 3D-Var scheme, which means that the lateral boundary conditions can be used either from the intermediate limited area model (ALADIN/LACE) or from the global model (ARPEGE).

These general experiments have led us to conclude, that the optimal choices for the ALADIN/HU model using the 3D-Var scheme are: the lateral boundary conditions to be provided by the same integration of the coupling model, thus the information is consistent in time, digital filter initialization to be applied both in cycling and production, in order to have a filtered forecast, and finally, the choice of the lateral boundary conditions from the global or limited area model is not so important.

In view of these results, it was decided to continue the experiments with the 3D-Var scheme, for some individual synoptic cases. In that regard two case studies have been presented. In the first one, the operational model did

not predict a heavy rainfall, which happened over the Danubian Basin. It has been tried to demonstrate, how the assimilation of observations can improve the operational forecast. The results of different integrations of the model have been compared, and they revealed that the model using the 3D-Var scheme has a clear advantage over the dynamical adaptation. The location of the rainfall has been well predicted, however, the quantity of precipitation was overestimated. Since both models were using the same lateral boundary conditions, it means that the observations and data assimilation algorithm are responsible for the improvements of the model with the 3D-Var scheme. The second case presents the disastrous floods, which hit Austria, Germany, and the Czech Republic, in August 2002. Large amount of precipitation, more than 100 mm/24h, was measured in different locations. The intensive rainfall has been well predicted by the operational model, both as location and amount, which made us to conclude that the information from the coupling model was accurate. The results of the model using the 3D-Var scheme were investigated, and showed that the forecasts have been in accordance with the reality. Both models have been predicted areas with huge amount of rain and high humidity, which have the same pattern. Therefore, beside the accurate information from the lateral boundary conditions, the ALADIN/HU model using the 3D-Var scheme with some additional local measurements was performing equally well as the global 4D-Var data assimilation system of the ARPEGE model.

The two case studies highlighted that the information from the lateral boundary conditions should be accurate, in order to obtain a good short-range forecast. Also it has been presented that the current 3D-Var scheme benefits from the assimilation both of the surface observations and radiosounding data.

This paper emphasizes that the present framework of the ALADIN/HU 3D-Var system is appropriate to obtain an improved forecast. In the future, it is planned to try other background error statistics (computed by the lagged NMC constant coupling method or the ensemble method), more other types of observations to be assimilated (for instance, aircraft or satellite observations), and to obtain the first guess by using a simple, explicit blending algorithm.

Acknowledgements—This work was made possible thanks to the financial support provided through the European Community's Human Potential Programme under contract HPRN-CT-1999-00057, ALATNET. ALATNET is supported by the TMR/IHP Programme of the European Community, but the information provided here is the sole responsibility of the ALATNET team and does not reflect the Community's opinion. The Community is not responsible for any use that might be made of data appearing here. The authors are grateful to all the colleagues from the ALADIN community, who have contributed to the development of the data assimilation algorithms within the ALADIN model. Special thanks to *Claude Fischer* and *Loïk Berre* for fruitful discussions and collaboration. The first author would like to thank the 3D-Var team from the Hungarian Meteorological Service, for their useful advices. The support of the National Meteorological Administration of Romania was very much appreciated by the first author.

References

Alexandru, S., 2002: 3D-VAR data assimilation experiments for the double-nested limited area model ALADIN/Hungary. *ALATNET Internal Note* (http://www.cnrm.meteo.fr/alatnet/).

Alexandru, S., 2003: Further experiments with the 3D-VAR data assimilation scheme for ALADIN/Hungary model. *ALATNET Newsletter* 6 (http://www.cnrm.meteo.fr/aladin/-newsletters/news23/news23-6.html).

Berre, L., 2000: Estimation of synoptic and mesoscale forecast error covariances in a limited area model. *Mon. Weather Rev. 128*, 644-667.

Courtier, Ph., Freydier, C., Geleyn, J.-F., Rabier, F., and *Rochas, M.*, 1991: The ARPEGE project at Météo-France. *ECMWF Seminar Proceeding*, Reading, Vol. II, 193-231.

Davies, H.C., 1976: A lateral boundary formulation for multi-level prediction models. *Q. J. Roy. Meteor. Soc. 102*, 405-418.

Sopko, 2003: Model predictions of the floods in the Czech Republic during August 2002: The forecasters' erspective. *ECMWF Newsletter* 97, 2-6 (http://www.ecmwf.int/publications/-newsletters/pdf/97.pdf).

Gilbert, J.C., and *Lemaréchal, C.*, 1989: Some numerical experiments with variable storage quasi-Newton algorithms. *Math. Prog. B25*, 407-435.

Horányi, A., Ihász, I., and *Radnóti, G.*, 1996: ARPEGE/ALADIN: A numerical weather prediction model for Central-Europe with the participation of the Hungarian Meteorological Service. *Időjárás 100*, 277-301.

Pailleux, J., 1997: 1987-1997: Ten years of research and operational activities with the Integrated Forecasting System (IFS). *ECMWF Newsletter* 75, 2-7 (http://www.ecmwf.int/publications/-newsletters/pdf/75.pdf).

Parrish, D. and *Derber, J.*, 1992: The National Meteorological Center's spectral statistical interpolation analysis system. *Mon. Weather Rev. 120*, 1747-1763.

IDŐJÁRÁS

Quarterly Journal of the Hungarian Meteorological Service
Vol. 109, No. 4, October–December 2005, pp. 257–279

Development of regulatory transmission modeling in Hungary

Dezső Szepesi[1]*, Katalin Fekete[1], Richárd Büki[2], László Koncsos[3] and Endre Kovács[4]

[1]*Consultants on Air Resources Management (CARM) Inc., Katona J. u. 41, V/25, H-1137 Budapest, Hungary; E-mail: szd12506@ella.hu*

[2]*Meteorological Service of the Hungarian Defence Forces, P.O. Box 1885, Budapest, Hungary*

[3]*University of Technology and Econimics, Műegyetem rkp. 11, H-1111 Budapest, Hungary*

[4]*Ministry of Environment and Water Management, P.O. Box 351, H-1394 Budapest, Hungary*

(Manuscript received in final form September 15, 2005)

Abstract—The paper describes the four-decade development of theoretical and practical steps (correct mathematical and atmospheric-physical simulation, temporal and spatial representativity of input data, scrutinised QA/QC, testing and validation, model comparison exercise) carried out to achieve a new regulatory model called HNS-TRANSMISSION for Hungary. Results of climatological assessments of meteorological input parameters (surface wind and atmospheric stability) and maps of base level urban and regional air pollution are also presented.

Key-words: base level air pollution, regional scale wind field, Szepesi-type stability categories, temporal and spatial representativity of meteorological data.

1. Introduction

Air quality modeling in Hungary have been developed in close co-operation among meteorologists, engineers, and project managers of national authorities. This work was helped by numerous able colleagues and technicians of the Department of Atmospheric Environment at the Hungarian Meteorological Service, later at CARM, Budapest, Hungary for many decades. Before 1960,

* Corresponding author

similarly as in other parts of the world, mostly public health people carried out air pollution surveys in Hungary, and some of them was even engaged in stack height calculations.

The ambient air in Hungarian cities before the 1980's was rather polluted, mostly due to solid fuel burning in individual stoves and to the exhaust gases of outdated car engines. *Fig. 1* shows the 50-year trend of air pollutant concentrations in ambient air of Budapest. Breaks in SO_2 curve are due to changes of sampling and evaluation methods (*Fehér* and *Szepesi*, 1970).

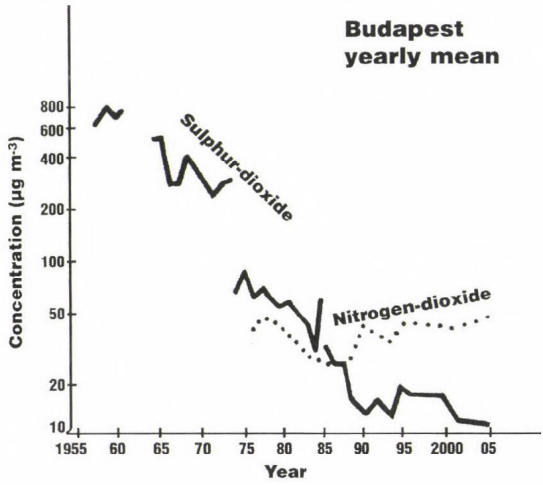

Fig. 1. 50-year trend of air pollutant concentrations in ambient air of Budapest.

At the beginning of the environmental conscious era (around 1970), project managers of national authorities worked out an effective air pollution abatement strategy for cities, including transition from solid fuel to natural gas, and from individual stoves to central and district heating. Heavy industry was placed out of the inner part of cities. This resulted in a considerable drop of SO_2 and soot concentrations soon. Parallel to this effort, intensity and duration of the London-type smog situations considerable dropped (see *Table 1*).

Meteorologists were also active in these decades helping authorities in finding the necessary dimension of abatement strategy. Director of the Hungarian Meteorological Service established a research group for air pollution studies, and a scientist was sent to the US Weather Bureau as a UN fellow for one year to be familiarized with the whole spectrum of air pollution meteorology in 1964. The fellow visited 27 research establishments in the US, but the most profitable 3 months were spent at the US Weather Bureau

Research Station (R.A. Taft Center) in Cincinnati, Ohio. Here he took part in field measurements, theoretical and applied researches. In cooperation with American experts, the basis of the first generation transmission system was established (see *Table 2*).

Table 1. Most severe smog situations in Budapest, $\mu g\ m^{-3}$

Period with smog	SO_2	Soot	NO_2
1936–38, winter mean (*Waldbauer,* 1938)	–	1070	–
March 16, 1959	3500–4500	5400	–
January 21–23, 1970	1500–1800	1000	–
January–February, 1989; 55 days	200–670	8–350	20–200

During his stay in the USA, diffusion climatological investigations were carried out in Hungary for the period of 1959–63 by punch card technique for wind and atmospheric stability conditions. Mixing height conditions were evaluated, and the first generation model was programmed some years later.

In 1974, the second generation transmission model system named ISAQA was validated for a large power plant at Pécs, south Hungary. The project was ordered by the Ministry of Environment in cooperation with the public health authorities). SO_2 concentrations were measured for a year at 32 stations, surface wind was observed at 6 points, upper air was investigated by pilot balloons, lapse rate conditions were calculated using orographic temperature gradient measurements. Measured and calculated concentration values were in satisfactory correlation. Based on these results, the Ministry on Environment started to fine heavy polluting industrial sources, the first time in Hungarian history.

Description of this model (its acronym is ISAQA) is listed in the Compendium of Regulatory Air Quality Models, together with 182 other models collected worldwide in a program sponsored by the Climatological Commission of WMO, when the author served it as rapporteur of air pollution for 15 years (*Szepesi,* 1989). The model was applied for some hundreds of cases in three decades without any complains.

The third generation of this model, which was developed and programmed in an EOV space-informatical system was named as HNS-TRANSMISSION. It is one of the standardized models in Hungary endorsed by the European Environmental Agency.

Table 2. Specifications and phases of the 3-generation model development

Generation	Model characteristics	
	Main goal	**Considerations**
First generation 1960's	Establishment of regulatory transmission modeling for Hungary (*Szepesi,* 1964, 1967)	Local scale model for point/area-sources, climatologically correct transmission input data system
Second generation 1970's and 1980's	Standardization of the transmission system for Hungary (*Fekete et al.,* 1983). Long-range and acid rain model (*Fekete* and *Szepesi;* 1987)	Orography, chemistry, initial dispersion, deposition, continental, regional, and urban scale polluting effects
Third generation 1990–2005	Regulatory model according to new domestic and EU regulations (HNS-TRANSMISSION) (*present paper*)	New definitions according to the demand of recent regulations (*OGG,* 2001). Simulation of the effects of 50 separate sources. Line sources, plaza parking lots, model estimation of base level air pollution, automatic estimation of area of significant impact, surface and most frequent wind maps, transmission input data system for the whole country (152 small areas). Regional and urban base level air pollution maps from recent measurements

In 1994, Hungary took part in a model intercalibration exercise of the European nations in Belgium (*Cosemans et al.,* 1994). The most important 1 hour maximum concentrations, calculated by the Hungarian standardized model HNS-TRANSMISSION, were in good agreement with values estimated by other national models. This model in its final form contains five years of meteorological data matrices, ready to apply to 150 localities covering all of Hungary. Results of a domestic model comparison of the two standardized models (AERMOD-HNS/HNS-TRANSMISSION) can be found at the web site: www.levegokornyezet.hu. Further model intercalibration was taken in the framework of COST Action 710 WG4. (Harmonization of the pre-processing of meteorological data for atmospheric dispersion models, E.C. Cost Action 710-Final Report, EUR 18195 EN.)

2. *Mathematical considerations*

Recently, new EU-conform regulations on air quality (*OGG,* 2001–2004) were promulgated and endorsed for Hungary. To meet the requirements of these regulations, development of a new, a third generation regulatory model system, named HNS-TRANSMISSION (domestic name TRANSZMISSZIÓ 1.1), was necessary. This article is to present major developments achieved.

We have introduced, among others, a new definition, called average concentration for the actual sector, which is similar to the most probable concentration, but refers to a narrower sector (*Fig. 2*). The difference is in the definition of the borders of the sector. In the new definition we use the concept of *Meade* and *Pasquill* (1958), that means that the borders of the sector are at the lines of the 10-percents value of the ground-level centerline concentration.

It will be shown, that this newly introduced definition can be simply estimated by multiplication of the ground-level centerline concentration by a constant. Finally, we introduce a factor which is vital of estimating the exceedences of 1-hour maximum concentration limit value.

Let us see the basic definition we should use, introducing the concept of the average concentration for the actual sector. The concentration is assumed to have Gaussian distribution. The well known and the new definitions of different types of concentrations and other related parameters are shown in *Fig. 2.*

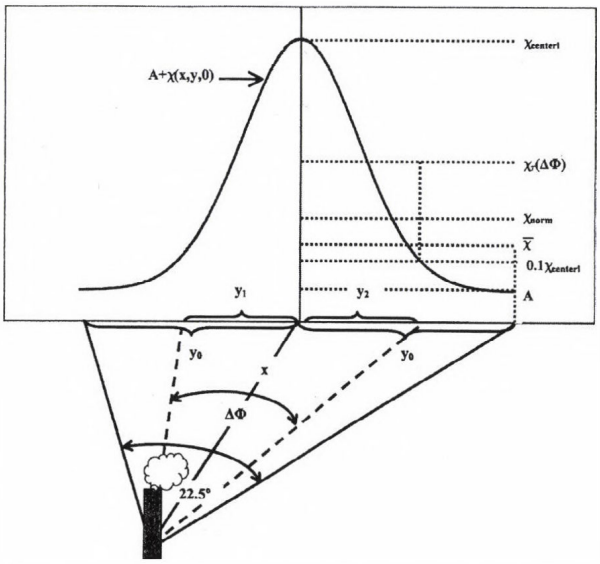

Fig. 2. The Gaussian distribution and the scheme of different types of estimated concentrations.

2.1 Ground-level concentration from an elevated point source

This well-known Gaussian formula specifies the concentration at the ground level along the downwind distance x from the source point:

$$\chi(x,y,0) = \frac{E}{\pi \sigma_y \sigma_z u_h} e^{\left(-\frac{H^2}{2\sigma_z^2}\right)} e^{\left(-\frac{y^2}{2\sigma_y^2}\right)}, \quad (1)$$

where

$\chi(x,y,0)$: concentration, μg m^{-3},
(x, y, z): receptor locations, m,
x: downwind distance from source to receptor, m,
y: crosswind distance, from source to receptor, m,
z: height above the ground, m,
E: pollutant emission rate, μg s^{-1},
σ_y: dispersion coefficient in the crosswind direction, m,
σ_z: dispersion coefficient in the vertical direction, m,
u_h: wind speed at the source-height, m s^{-1},
H: effective height of the stack, m,
A: base level air pollution.

2.2 Ground-level centerline concentration from an elevated point source

This is a special case of Eq. (1) when $y=0$.

$$\chi_{centerl} = \chi(x,0,0) = \frac{E}{\pi \sigma_y \sigma_z u_h} e^{\left(-\frac{H^2}{2\sigma_z^2}\right)}. \quad (2)$$

This type of maximum concentration occurs rarely, but according to the new air quality regulation (*OGG,* 2001–2004), this has to be taken into account for determining the area of significant impact (ASI) in environmental impact assessments (EIA) (see section 4).

2.3 The most probable concentration

This definition is also introduced by *Fekete et al.* (1983):

$$\overline{\chi_\tau} = \frac{1}{2y_0} \int_{-\infty}^{+\infty} \chi_{centerl}\, e^{\left(-\frac{y^2}{2\sigma_y^2}\right)} dy = \frac{\chi_{centerl}\sqrt{2\pi}}{2y_0}\sigma_y = \tag{3}$$

$$= \sqrt{2\pi}\left(\frac{1}{2y_0}\chi_{centerl}\,\sigma_y\right),$$

where

$\overline{\chi_\tau}$: most probable concentration, μg m^{-3},

y_0: crosswind length belonging to the meteorological wind sector (22.5°), m,

$\chi_{centerl}$: the ground-level centerline concentration, as defined in Section 2.2, μg m^{-3}.

The other expressions used are the same as before.

This type of formula is used in the model for estimation of yearly mean ground level concentration.

2.4 Average concentration for the actual sector

Based on the suggestion of *Meade* and *Pasquill* (1958), we define this type of concentration distribution. The average concentration is the integral between the 10-percents limits of the ground-level centerline concentration. $\Delta\Phi$ is the angle between the two 10-percent isolines of the ground-level centerline concentrations.

In the first step we calculate the limits of the integral, which, in the previous case, was $\pm\infty$. Because of symmetry case, $y_1 = y_2$, the basic equations are

$$\begin{aligned} &\chi(x,y,0) = 0.1\chi(x,0,0), \\ &y_{1,2} = \pm\sigma_y\sqrt{2\ln(10)} \approx \pm 2.15\sigma_y\,, \\ &2y_1 = 2y_0 \approx 4.30\,\sigma_y, \end{aligned} \tag{4}$$

where y_1, y_2 is crosswind distances belonging to borders of sector $\Delta\Phi$, m.

Resulting from this transformation, we have got the average concentration for the actual sector ($\Delta\Phi$). With help of the Taylor-series and the definition of the exponential function the following equation can be derived from Eqs. (3) and (4):

$$(\overline{\chi_\tau})_{\Delta\Phi} = \frac{1}{2y_0} \int_{-2.15\sigma_y}^{+2.15\sigma_y} \chi_{centerl}\, e^{\left(-\frac{y^2}{2\sigma_y^2}\right)} dy = \frac{1}{2y_0} \chi_{centerl} \int_{-2.15\sigma_y}^{+2.15\sigma_y} e^{\left(-\frac{y^2}{2\sigma_y^2}\right)} dy \approx$$

$$\approx 2.44 \left(\frac{1}{2y_0} \chi_{centerl}\, \sigma_y \right) = 1.22 \frac{\chi_{centerl}\, \sigma_y}{y_0}. \tag{5}$$

This derivation is correct, because σ_y (and σ_z, respectively) is the function of x and not of y, so it can be considered as constant (*Fekete et al.*, 1983).

Comparing Eq. (3) to Eq. (5), we can see that the difference between the concentrations calculated between $\pm\ \infty$ and between the borders suggested by *Meade* and *Pasquill* (1958) is negligible, it is only about 2.7%.

Substituting y_0 from Eqs. (4) and (5) we got:

$$(\overline{\chi_\tau})_{\Delta\Phi} = 0.57\, \chi_{centerl}\,. \tag{6}$$

The multiplication factor is constant, 0.57, because the crosswind dispersion parameter (σ_y) effects $\chi_{centerl}$ and y_0 similarly, so at the simplification of the equation it falls out. The reason for determining Eq. (6) and the average concentration for the actual sector is that the frequency of wind direction in the meteorological wind sectors (which are 22.5° wide) are available as climatologic data in Hungary, and not as the frequency of a certain direction by degrees. When the wind is not exactly in one of the usual wind sectors, and usually it is not, then we can estimate the climatologic frequency of the certain wind direction through weighting using the available information. This method can be adapted for planning purposes easily.

This is the critical formula used by Hungarian environmental inspectors to qualify whether a source complies with limit values and allowable limit value exceedences, or not.

Area sources were treated by an algorithm (*Szepesi*, 1972), its graphical scheme is shown in *Fig. 3*.

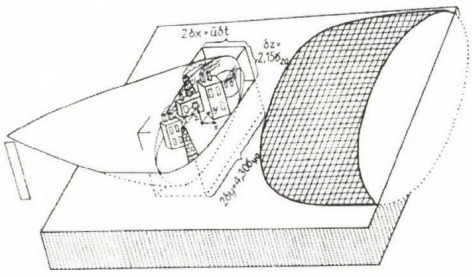

Fig. 3. Scheme of the initial dispersion (area or diffuse sources).

The correct estimation of exceedences of the limit values is vital for air resources management, air quality control, and air quality planning. If we calculate the 1-hour concentration and the base level air pollution, we should divide this sum by a factor denoted by e. So the yearly number of cases, ($Nt(w,x)$), when concentration is above the limit value, is the function of wind direction, w, downwind distance, x, wind speed, u, and atmospheric stability, S, beside of the source parameters:

$$Nt(w,x)=\left\{\left[\sum_u\sum_S\left(\frac{f^{N1}_{w,u,S}}{e^{N1}}\right)\right]-a\right\}+\left[\sum_u\sum_S\left(\frac{f^{N2}_{w,u,S}}{e^{N2}}\right)\right], \tag{7}$$

where

$f^{N1}_{w,u,S}$: the number of cases, when the sum of the ground-level concentration and base level air pollution is over the 1-hour limit value with a tolerable degree,

$f^{N2}_{w,u,S}$: the number of cases, when the sum of the ground-level concentration and base level air pollution exceeds the 1-hour limit value more than tolerable,

a: number of cases with allowable exceedences,

e^{N1}, e^{N2}: factors of normalization to divide the number of cases to $f^{N1}_{w,u,S}$ and $f^{N2}_{w,u,S}$.

Practically the factor e is the ratio of the crosswind width of the 22.5° sector and that of the sector, where the concentration is greater than the limit value. Starting from this principle, the factor e cannot be less than 1. The value of e varies between 1 and 21 depending on the meteorological and physical conditions, such as emission rate, source parameters, temperature of the ambient air, etc.

An algorithm can be deducted for the factor e. Considering the geometry of *Fig. 2* and the definition of the factor e:

$$\begin{aligned} e&=\frac{2y_0}{|y_1|+|y_2|}=\frac{y_0}{|y_1|},\\ y_0&=x\left(\frac{11.25^\circ\pi}{180^\circ}\right). \end{aligned} \tag{8}$$

The inequality, which has to be solved, is:

$$\chi_{norm} \leq \chi(x,y,0) + A \ , \tag{9}$$

where χ_{norm}: 1-hour mean limit value of concentration, μg m^{-3},
A: base level air pollution, μg m^{-3}.

After transformations and defining the χ_A as the difference below:

$$\chi_A = \chi_{norm} - A \ ,$$

Eq. (9) has the form:

$$\chi_A \leq \chi(x,y,0) \, .$$

Let us define a source type factor Q, as:

$$Q = \frac{E}{\pi \sigma_y \sigma_z u_h} \tag{10}$$

We obtaine:

$$y_1 = \pm \sqrt{\left| 2\sigma_y^2 \ln\left(\frac{Q}{\chi_{norm} - A} \right) - H^2 \left(\frac{\sigma_y}{\sigma_z} \right)^2 \right|} \, . \tag{11}$$

Because only the positive resolution of Eq. (8) has physical meaning, we obtain the following algorithm for the e factor:

$$e = \frac{x\left(\frac{11.25^\circ \pi}{180^\circ} \right)}{\sqrt{\left| 2\sigma_y^2 \ln\left(\frac{Q}{\chi_{norm} - A} \right) - H^2 \left(\frac{\sigma_y}{\sigma_z} \right)^2 \right|}} \, . \tag{12}$$

3. Representative meteorological input data

3.1 Temporal representativity

For long-term planning purposes, it is important to apply meteorological parameters evaluated from data of 30 or 100 years long measurements, or by using shorter, but climatologically representative (normal) 3–5 years long data series.

To investigate this problem on a more objective way, a study of the Péczely-type macrosynoptic situations was carried out (see the web site www.levegokornyezet.hu/climatic aspects) for the period 1881–2001 for Hungary by using the following algorithm:

$$T = \overline{\left(\frac{(y_i - Y_i)^2}{D_i^2} \right)}, \qquad i=1,2,3,...,13,$$

where

T: rate of closeness,

i: index of 13 macrosynoptic situation types,

y: frequency in a specific year,

Y: mean frequency for a reference period,

D^2: standard deviations for the whole reference period,

Upper bar denotes averaging for all i indices.

Table 3 presents the deviations of each year from the 1881–2001 mean, based on the frequency of occurrence of Péczely-type macrosynoptic situations.

By applying this algorithm, 1995, 1997, and 1998 can be considered as the most normal years in the latest decades, and the least normal years were 1981, 1983, and 1996.The mean climatological representativity index of the meteorological data of the 1959–1963 period (the transmission base of the HNS-TRANSMISSION model) was 1.07, which is in the range of 0.372–3.251, and can be considered representative.

In an earlier study (*Szepesi et al.*, 1993), it was also shown, that this base data period (1959–63) approximates the average macrosynoptic situation frequency satisfactoryly (mean deviation=1.0, standard deviation=0.57), much better than other periods considered. As a conclusion we can say, that the view of some researchers, that data from the latest years are the most relevant, is not acceptable, it could be extremely misleading in certain cases. The method presented is able to take into account the quantitatively hypothetical changes of climatic regimes, too.

3.2 Regional representativity

The basic idea of meteorological data pre-processing is that for ground-level concentration estimations it is more representative to use regional scale meteorology – in other words, average meteorology for an area of 20–30 km in diameter – instead of measurements made at a single point. This is called

spatial representativity or regionalization of meteorological data. The method of data regionalization is described by *Fekete et al.* (1983), here we only summarize the main lines.

Table 3. Order of climatological representativity

Year	Representativity index for the most normal years	Year	Representativity index	Year	Representativity index	Year	Representativity index for the least normal years
1978	0.296	1987	0.699	1964	0.933	1961	1.154
1955	0.311	1985	0.706	2000	0.933	1975	1.155
1957	0.335	1896	0.708	1970	0.934	1929	1.164
1931	0.372	1908	0.723	1910	0.935	1907	1.165
1927	0.378	1934	0.729	1990	0.960	1923	1.175
1995	0.403	1912	0.745	1952	0.997	1958	1.177
1997	0.405	1913	0.746	1884	1.004	1963	1.203
1998	0.406	1926	0.747	1930	1.007	1991	1.216
1891	0.427	1894	0.749	1890	1.009	1966	1.219
1988	0.431	1992	0.752	1968	1.013	1984	1.225
1994	0.453	1909	0.759	1901	1.017	1976	1.238
1940	0.470	1893	0.760	1999	1.019	1932	1.240
1993	0.473	1954	0.761	1898	1.032	1945	1.245
1886	0.497	1917	0.766	1960	1.039	1887	1.252
1922	0.503	1950	0.780	1911	1.039	1967	1.259
1897	0.503	1979	0.781	1904	1.041	1969	1.286
1892	0.534	1986	0.809	1936	1.050	1972	1.327
1889	0.544	1883	0.822	1905	1.054	1933	1.336
1971	0.549	1925	0.831	1959	1.054	1921	1.443
1948	0.555	1956	0.832	1918	1.067	1982	1.496
1973	0.563	1947	0.834	1989	1.073	1938	1.539
1965	0.570	2001	0.835	1919	1.081	1916	1.585
1935	0.583	1943	0.856	1915	1.095	1944	1.597
1888	0.593	1962	0.860	1953	1.102	1996	1.615
1937	0.647	1942	0.865	1980	1.106	1983	1.625
1881	0.649	1974	0.880	1885	1.114	1946	1.968
1951	0.653	1924	0.883	1903	1.120	1939	2.012
1977	0.674	1928	0.893	1906	1.122	1900	2.050
1882	0.683	1949	0.916	1941	1.124	1920	2.252
1895	0.688	1914	0.922	1902	1.136	1981	2.466
						1899	3.251

3.3 Wind conditions

The aim of establishing wind maps is to furnish readily available regionally and temporally representative wind statistics for any location in the country, for environmental impact assessments. For the analysis of these, all available surface wind data series (more than 300 between 1881 and 1980) and upper air ascents (22 long series between 1929 and 1989) in Hungary were considered (*Szepesi* and *Fekete*, 1993).

This wind is representative for quasi-level terrain of average roughness without obstacles. The local effects of extreme roughness, sheltering by obstacles and mountainous terrain must be model-corrected.

Validation of the wind mapping concept gave satisfactory results. It also revealed many inconsistencies in the locating of instruments and former manual evaluation of wind record-charts. However, it also confirmed and quantified some previous findings, for example, that the frequencies of the westerlies and easterlies over the country are considerably increased by orographic channeling of the North Carpathian Mountains.

This is a non-computerized (graphical) data assimilation technique. After plotting all wind direction and speed data available (sixteen directions, and mean speed data for each direction, respectively), we can analyze these charts graphically, one by one (see *Figs. 4* and *5*). These maps make possible to pick up or interpolate yearly average wind direction frequencies and mean speed value data at any point of the country.

The last step is to apply the circular polar smoothing process presented by *Tar* (1991), then to use an interpolation technique built in the HNS-TRANSMISSION model to interpolate transmission data matrices to any point of interest over the country.

Transmission matrices, gained this way and built in the HNS-TRANSMISSION model, will be temporally and spatially representative and serve as readily applicable input database.

3.3.1 Most frequent winds

Evaluation of the most frequent meteorological situation was another important task. This was carried out in the following way. Since atmospheric stability category $S=6$ (Szepesi stability 1–7, see *Fekete et al.*, 1983) is the most frequent one, surface wind speed prevailing during this stability conditions were evaluated over Hungary. The numerical values ranged from 1.6 m s^{-1} to 3.1 m s^{-1} (see *Fig. 9h*). These parameters are essentials for the estimation of the area of significant impact (ASI) according to *OGG* (2001–2004).

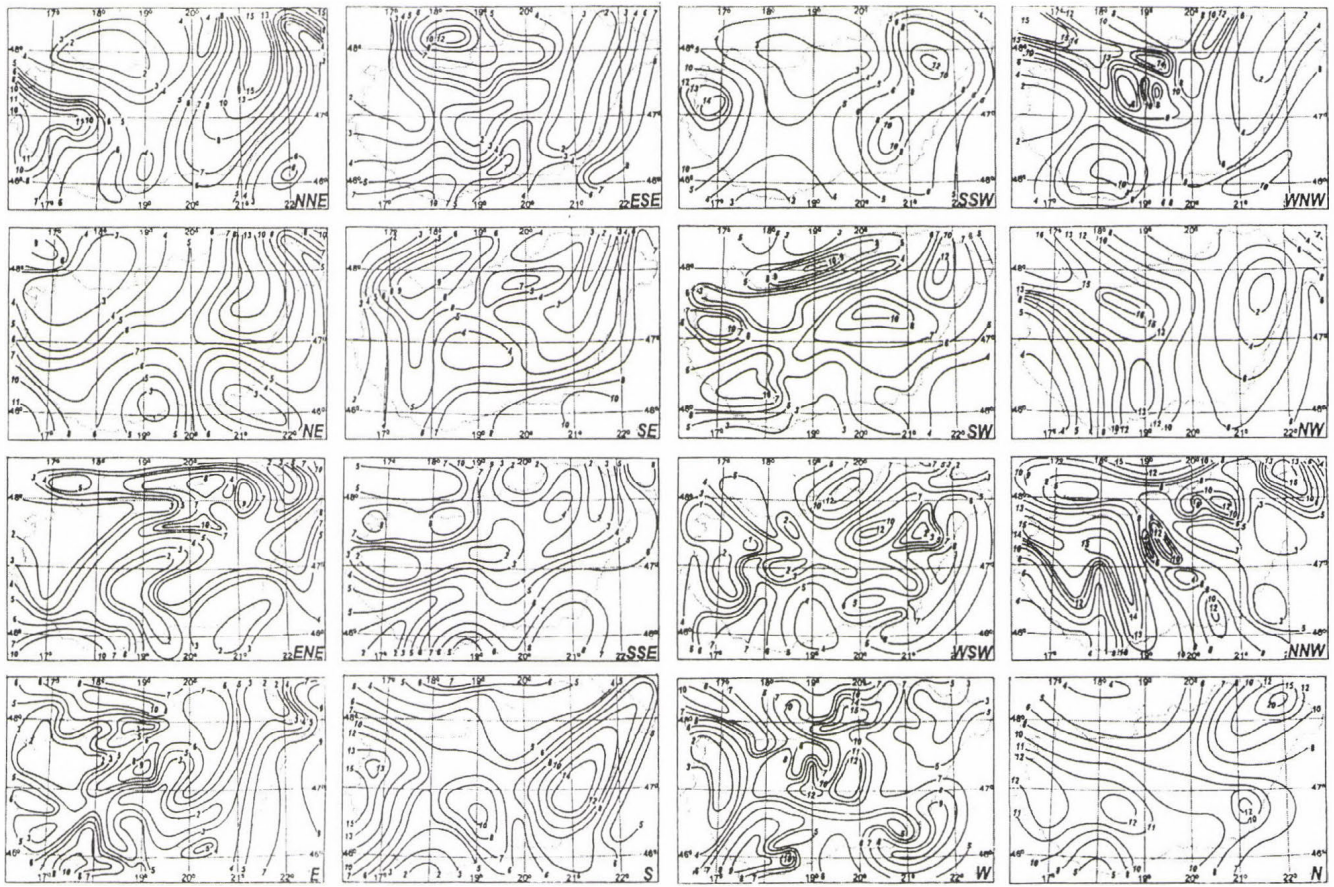

Fig. 4. Relative frequencies of surface wind direction in Hungary (1880–1990), %.

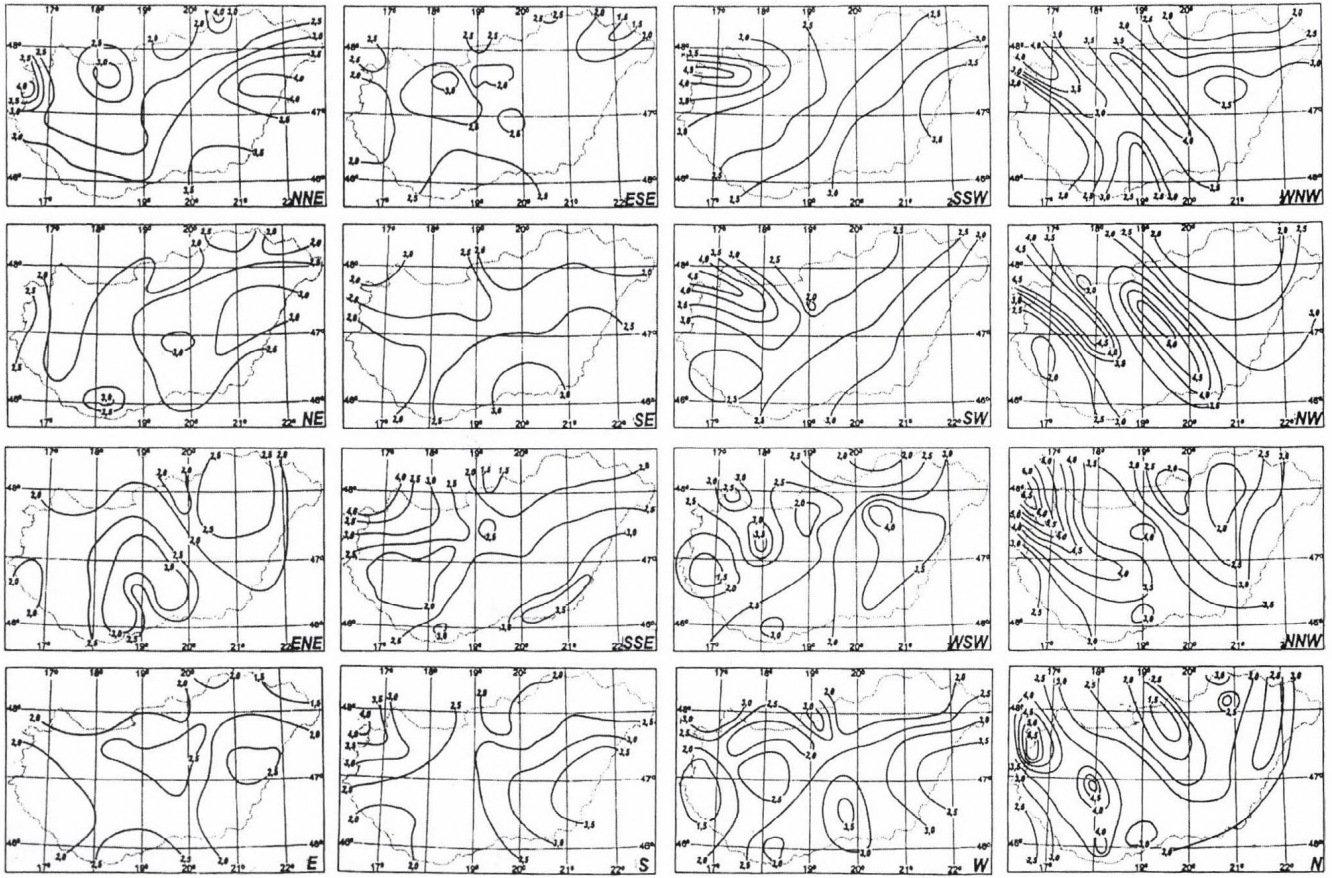

Fig. 5. Mean surface wind speed in Hungary (1880–1990), m/s.

3.4 Stability conditions

Atmospheric stability is estimated in Hungary for low sources by the Pasquill-Gifford-Turner (PGT) procedure, and for medium and high sources by the Szepesi method (*Szepesi,* 1967), based on classification of temperature lapse rates of the lowest 300 m layer. The climatology of the lapse rates is shown in *Fig. 6.* Frequency distributions were analyzed based on six daily radiosonde ascents between 1959 and 1963, resulting in a very characteristic and smooth pattern *(Szepesi et al.*, 1993).

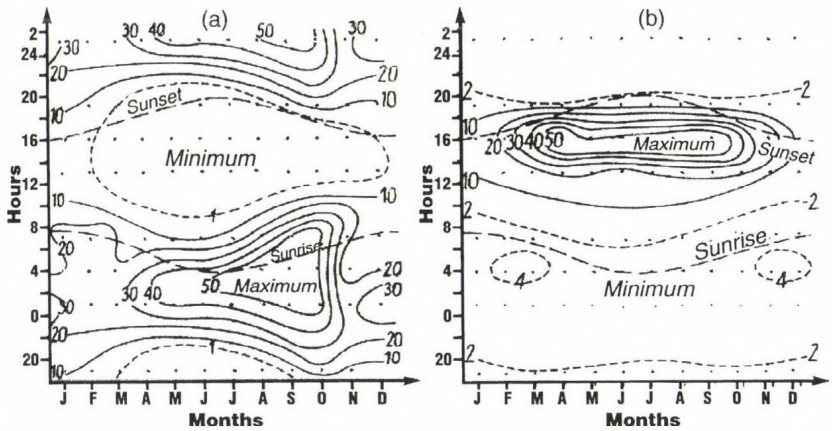

Fig. 6. (*a*) Relative frequency (%) of stable (S=1, 2, 3) and (*b*) superadiabatic (S=7) stratification of the lowest 300 m layer (1959–1963) over Budapest.

By using PGT or Szepesi-type stability classes, dispersion coefficients σ_y and σ_z were determined by the *Nowicki* (1976) formulas.

For deeper air layers, the exponent p and the stability indicators must be transformed using the diagram shown in *Fig. 7.* This diagram was constructed using a long series of temperature data measured on high meteorological towers and radiosondes.

3.5 Transmission matrices

Multidimensional transmission matrices are the input bases for long-term estimates of pollutant concentrations *(Szepesi et al.*, 1967, 1985). They were established first time for 40 synoptic stations for the period 1959–1963 in Hungary.

The next step is to pre-process the transmission matrices based on 5 years of measurements. This period (1959–1963) was selected because of having similar weather characteristics as those of the 100 years period (1880–1980). In other words, the frequency distribution of macrosynoptic (Péczely) weather types were nearly similar in both periods.

For low sources, they are based on surface wind direction (16 bins) and speed (7 bins) records, and PGT stability categories using 5 years of SYNOP data. For medium and high sources, 500 m level wind maps (pilot balloon and radiosound) were used, together with the stability conditions (7 bins) estimated on the basis of the lapse rate of the lowest 300 m layer. Between the 40 points for any location in Hungary, a transmission matrix can be interpolated by using statistics of wind maps (see *Figs. 4* and *5*).

For estimation of 24 h mean and maximum concentrations, time series of meteorological data for 7 regions were included.

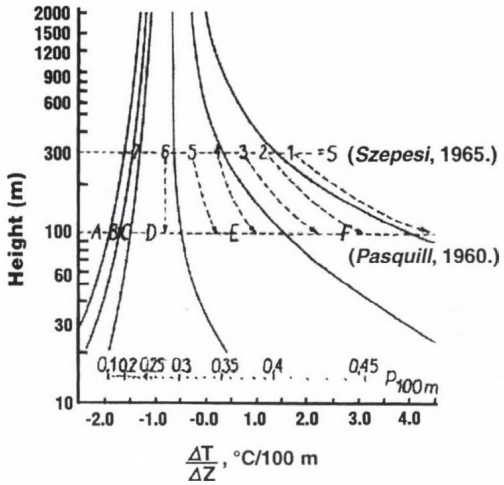

Fig. 7. Diagram for the transformation of wind profile equation exponent p and stability indicator S.

3.6 Background and base-level air pollution

3.6.1 Background pollution

Consistent estimation of background air pollution, originating from larger scale but less intense polluting sources, is of considerable importance for regulatory applications. Because of the very complex mechanisms involved, a practical simplifying approach was worked out (*Fig. 8*). By using this scheme,

contributions from global, continental, regional, and urban background pollution could be easily analyzed for any geographic locations. For local regulatory purposes, preparation of regional and urban background maps for the most important pollutants at 3-year intervals seems reasonable. The maps should be drawn based on all available measured data at urban and regional background stations and analyzed in the light of model estimated concentration patterns calculated using the relevant emission inventory and meteorological input.

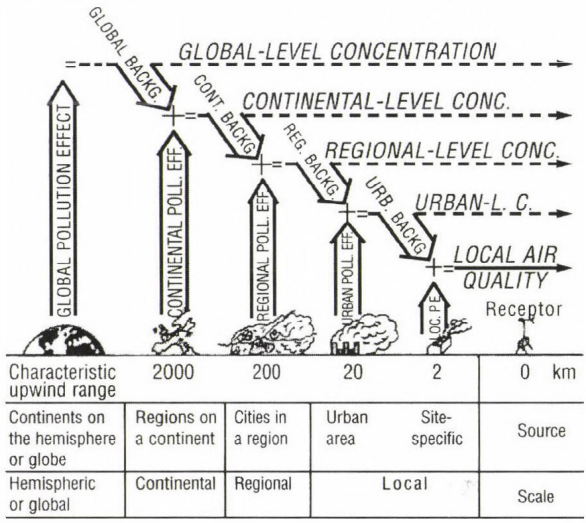

Fig. 8. Hierarchy of air pollution scales.

3.6.2 Base level air pollution

In conformity with Hungarian Clean Air Act Regulations (*OGG,* 2001–2004), it is necessary to introduce the concept of Base Level Air Pollution (BLAP), which is practically the long-term (yearly) average of background concentrations measured or estimated on a wider area around the planned source. It is an important parameter of any environmental impact assessments, and it is useful if it is available in advance.

Practical steps of its evaluation in the light of recent Clean Air Act regulations is described on the web-site www.levegokornyezet.hu. BLAP fields were estimated in a separate project, and maps presented here are possible examples of future official work.

There are two types: regional and urban BLAP maps.

- The regional BLAP maps were estimated for SO_2 and NO_2 by plotting all measured air pollution data available in Hungary for 1986–90. For the territorial analyses, emission inventories of SO_2, NO_2, and NH_3 were used (*Figs. 9 a-b*). For the total acid depositions maps, Acid Rain Model (*Fekete* and *Szepesi*, 1987) was run (see *Fig. 9d*).

  The PM_{10} regional map was estimated by the latest version of EMEP Eulerian Unified Model System for 2003 (*MSC-W Data Note 1*, 2004). For model calculations updated, received emission data were used. As *Fig. 9c* shows, regional PM_{10} BLAP for Hungary is 10 $\mu g\ m^{-3}$, and the number of days with limit value exceedencies in Budapest agglomeration is yearly 10. Preliminary model estimations show that over cities in Europe, where the share of diesel cars is over 70 percents (in Hungary it is 17%), exceedence days are close or above 35.

- Urban SO_2, NO_2, and CO BLAP maps for Budapest (see *Figs. 9 e-g*) were analyzed by *Vámos et al.* (2002). By the aid of the Budapest Public Health Institute, all measured high quality data were offered in processed form for 1998–2001. All urban measuring stations were visited and scrutinized. Parameters surrounding the stations, as building height, distance of nearby roads, street width, traffic intensity, and microclimatic characteristics were logged. These parameters are input data for model estimations. Direct impact polluting effect originating from nearby road traffic was subtracted from measured data. BLAP data gained this way were plotted and analyzed territorially by concentration isolines (see *Figs. 9 a-c*).

4. Model output

An example for the expected NO_x pollution around a new 2-source configuration, estimated by the model system HNS-TRANSMISSION, is shown in *Fig. 10*. The technical input data are emission rates (80 kg $NO_x\ h^{-1}$ and 200 kg $NO_x\ h^{-1}$), stack heights 20 m and 40 m, respectively, base level air pollution of 20 $\mu g\ NO_2\ m^{-3}$ (from *Fig. 9*), surface roughness of 0.5 m, most frequent wind speed of 2.5 $m\ s^{-1}$ (from *Fig. 5h*) and NO_x limit values of 200 $\mu g\ m^{-3}$ (1 h) and 100 (24 h) $\mu g\ m^{-3}$.

To meet the requirements of present Hungarian air quality regulations (*OGG,* 2001–2004), the following concentration patterns are output: 1-hour maximum concentration (*Fig. 10a*), yearly number of estimated concentration exceedences (*Fig. 10b*), 24-hour maximum concentration (*Fig. 10c*), yearly mean concentration (*Fig. 10d*), and the area of significant impact (ASI) (*Fig. 10e*), which at condition (b) has the largest range of 11.5 km.

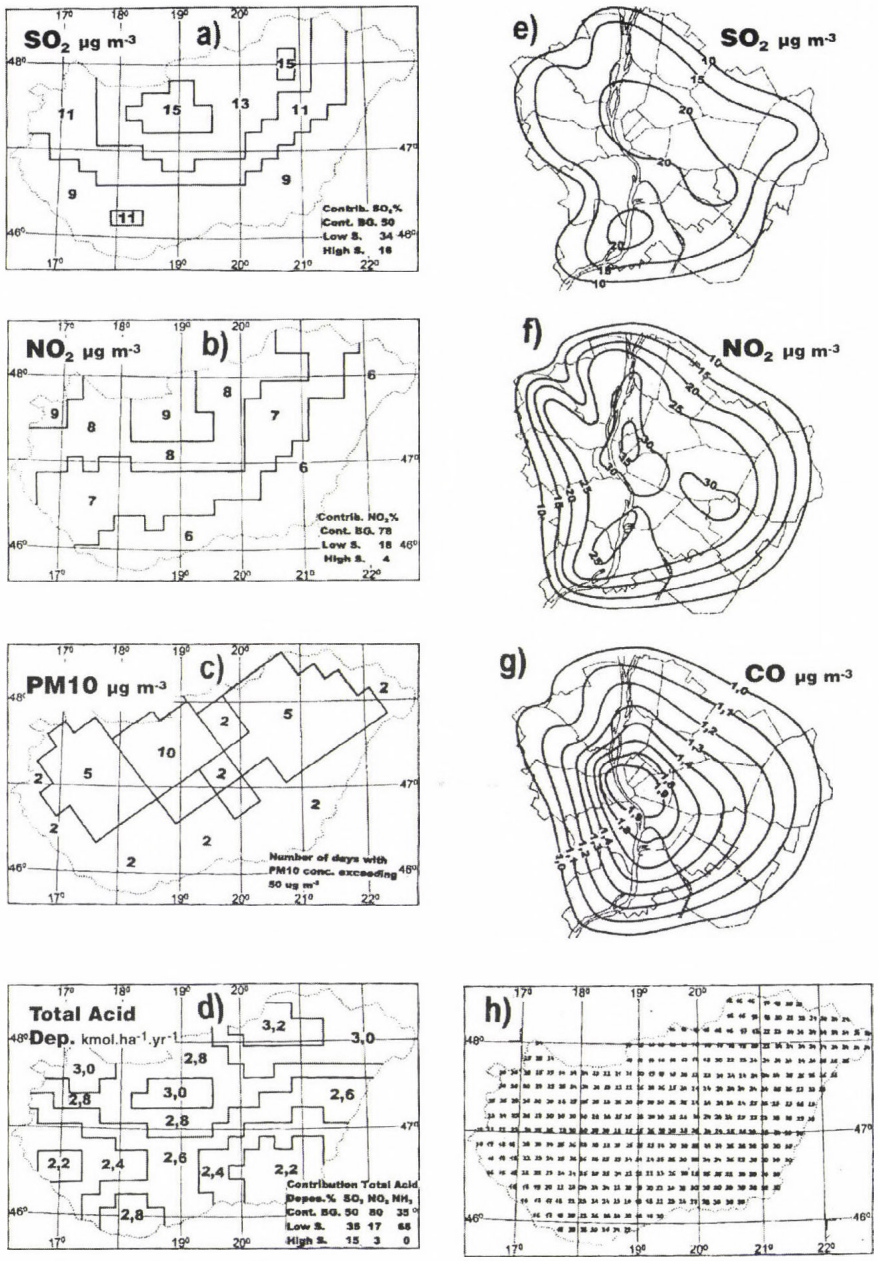

Fig. 9. Regional (*a*)–(*d*) and urban (*e*)–(*g*) base level air pollution and critical wind speed (*h*) over Hungary and Budapest.

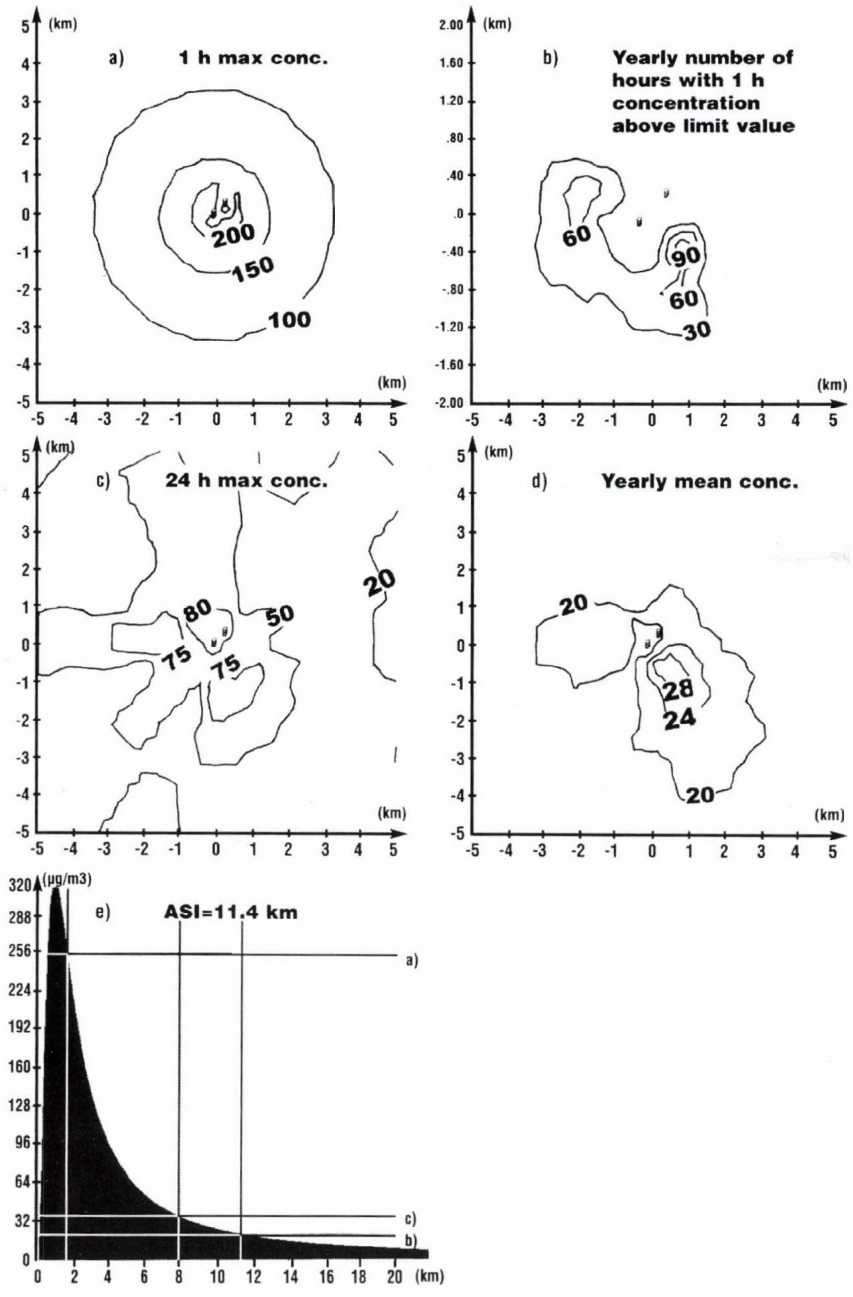

Fig. 10. Concentration distributions (*a*, *b*, *c*, *d*) and ASI (*e*) estimated by the HNS-TRANSMISSION model.

5. *Characteristics of model HNS-TRANSMISSION*

By using modules detailed in Section 2 and representative meteorological input data, regulatory model HNS-TRANSMISSION was prepared to satisfy the new regulations on air quality (*OGG,* 2001–2004). Major characteristics are the followings: the model estimates ground level concentration and deposition emitted by point and area sources – up to 50 sources –, located at different sites. It calculates 1 h, 24 h and yearly average, maximum values, and limit value exceedences. Their outputs are in tabled form or presented as territorial distributions on Unified Domestic Map System maps in selected colored forms. Dry deposition and chemical transformation modules are included as well.

Effects of inhomogeneous roughness, base level air pollution, and orographical effects in homogeneous or inhomogeneous distributions can also be easily simulated by the HNS-TRANSMISSION model.

Acknowledgements—Model development in Hungary was helped considerably by the successful programming work of *Domokos Szász, Iván Mersich, Lajos Gyenes, István Elekes,* and *László Koncsos*. Their contributions are highly appreciated.

References

Cosemans, G., Janssen, L., and *Maes, G.,* 1994: *The Third Workshop's Environmental Impact Assessment Model Intercomparison Exercise. Operational Short-Range Atmospheric Dispersion Models for Environmental Impact Assessment in Europe.* Mol, Belgium, 21-24 November 1994.

Fehér, V. and *Szepesi, D.,* 1970: Estimation of the allowable emissions for air pollution abatement program in Hungary. *Proc. of the Second International Clean Air Congress.* Washington D.C., December 10-14, 1970, 1081-1084.

Fekete, K., Popovics, M., and *Szepesi, D.,* 1983*: Guide to Estimate the Transmission of Air Pollutants* (in Hungarian). Orsz. Meteorológiai Szolgálat Hivatalos Kiadványai, LV, Budapest.

Fekete, K. and *Szepesi, D.,* 1987: Simulation of atmospheric acid deposition on a regional scale. *Environ. Manage. 24,* 17-28.

Meade, P.J. and *Pasquill, F.,* 1958: A study of the average distribution of pollution around Staythorpe. *Int. J. Air Pollut. 1, 60.*

Nowicki, M., 1976: Ein Beitrag zur Bestimmung universeller Diffusions-Koeffizienten. *Arch. Meteor. Geophis. A.,* No. 25, 31-45.

OGG, 2001-2004: *Official Government Gazettes* (Magyar Közlöny) (in Hungarian) 20/2001 (II.14), 21/2001 (II.14), 120/2001 (VI.30) and 4/2004 (IV.7), Budapest.

MSC-W Data Note 1, 2004: EMEP, Oslo.

Szepesi, D., 1964: A model for the long-term distribution of pollutants around a single source (in Hungarian). *Időjárás 68,* 257-269.

Szepesi, D., 1967: *Meteorological Conditions of the Turbulent Diffusion of Atmospheric Pollutants in Hungary* (in Hungarian). Orsz. Meteorológiai Intézet Hivatalos Kiadványai, XXXII, Budapest.

Szepesi D., 1972: Model for area sources (in Hungarian). *Időjárás 76,* 73-78.

Szepesi, D.J. (ed.), 1981: *Planning of the Atmospheric Environment* (in Hungarian). Műszaki Könyvkiadó, Budapest.

Szepesi, D.J., 1989: *Compendium of Regulatory Air Quality Simulation Models.* Akadémia Kiadó, Budapest.

Szepesi, D.J. and *Fekete, K.E.*, 1987: Background levels of air and precipitation quality for Europe. *Atmos. Environ. 21,* 1623-1630.

Szepesi, D.J. and *Fekete, K.E.*, 1993: Design wind maps for Hungary (in Hungarian). *Meteorológiai Tudományos Napok*, Magyar Tudományos Akadémia, Budapest.

Szepesi, D,J. Fekete, K.E., and *Gyenes, L.*, 1985: Regulatory models for environmental impact assessment in Hungary. *Int. J. Environ. Pollut. 5,* 497-507.

Szepesi, D.J., Szalai, S., and *Károssy, Cs.*, 1993: The climatological characteristics of the atmospheric environment (in Hungarian). *Magyar Meteorológiai Társaság, XXVII, Vándorgyűlés,* Debrecen.

Tar, K., 1991: *A Complex Statistical Analysis of Wind Climatology* (in Hungarian). Orsz. Meteorológiai Szolgálat Kisebb Kiadványai 67 sz., Budapest.

Vámos, A., Bobvos, J., Fekete, K., Szepesi, D., and *Titkos, E.*, 2002: Base level air pollution of Budapest (in Hungarian). CARM, Budapest, 1–12.

Waldbauer, O., 1938: The content of soot in the air of Budapest (in Hungarian). *Egészségügy 52,* 165-174.

BOOK REVIEW

J. R. Holton (editor-in-Chief), 2002: **Encyclopedia of Atmospheric Sciences**. Vol. 1-6. Elsevier Academic Press, 2780 pages, 1900 figures, maps, charts and photographs.

An encyclopedia (alternatively encyclopaedia) is a written compendium of knowledge. The term comes from the ancient Greek "enkuklios paideia" with the meaning "a circle of instructions" or "a well-rounded education", i.e., a repertory of wisdom young Greeks had to know on the seven liberal arts: grammar (science of language), rhetoric, dialectics (logic), arithmetic, astronomy, geometry, and music. Nowadays, an encyclopedia is either general or specializes in a particular field of studies.

A couple of years ago, Elsevier Academic Press started to publish a series of encyclopedias dealing with different fields of earth sciences. The *Encyclopedia of Volcanoes* and the four-volume set of the *Encyclopedia of Earth System Science* were published in 1999, the three-volume set of *Seas at the Millennium* and the five-volume set of the *Encyclopedia of Biodiversity* in 2000, the six-volume set of the *Encyclopedia of Ocean Sciences* in 2001, the six volumes of the *Encyclopedia of Atmospheric Sciences* in 2002, the ten-volume set of the *Treatise of Geochemistry* in 2003, the *Encyclopedia of Caves* and *Encyclopedia of Geology* in 2004. In the near future, two more encyclopedias will be published. The four volumes of the *Encyclopedia of Quaternary Science* are planned for 2006, the eleven volumes of the *Treatise on Geophysics* for 2007. The indicator of the series' success is not only the selling rates, but the title "Best Reference Source of the Year" from the Library Journal for the *Encyclopedia of Ocean Sciences* in 2001 and for the *Encyclopedia of Atmospheric Sciences* in 2002. *James Holton* editor-in-chief and his collaborators *John Pyle* and *Judith A. Curry* invited an enormous number of specialists from leading universities and research institutions from all over the world, for the formulation of the 350 entries. The entries of the encyclopedia cover all aspects of atmospheric sciences, including both theory and applications. It is an ideal resource for undergraduate and graduate students, active researchers, practicing meteorologists, climatologists, oceanographers, environmental scientists, ecologists, policy makers, and industrials to become acquainted with different atmospheric phenomena and to understand the relevance of the dynamical and physical processes of the atmosphere. An online version of the encyclopedia is also available for subscribers.

Gy. Gyuró

IDŐJÁRÁS

VOLUME 109 * 2005

BUDAPEST, HUNGARY

AUTHOR INDEX

Alexandru, S. (Bucharest, Romania) 233
Anda, A. (Keszthely, Hungary) 21
Ács, F. (Budapest, Hungary) 71
Bartholy, J. (Budapest, Hungary) 1, 217
Bencze, P. (Sopron, Hungary) 189
Bocheva, L. (Sofia, Bulgaria) 55
Büki, R. (Budapest, Hungary) 257
Cseh, S. (Győr, Hungary) 189
Dezső, Zs. (Budapest, Hungary) 217
Drucza, M. (Budapest, Hungary) 71
Fekete, K. (Budapest, Hungary) 257
Horányi, A. (Budapest, Hungary) 233
Hunkár, M. (Keszthely, Hungary) 39
Kerényi, J. (Budapest, Hungary) 205
Koncsos, L. (Budapest, Hungary) 257
Kovács, E. (Budapest, Hungary) 257
Labancz, K. (Budapest, Hungary) 157
Ladics, T. (Budapest, Hungary) 173
Lőke, Zs. (Keszthely, Hungary) 21
Marinova, T. (Sofia, Bulgaria) 55
Pongácz, R. (Budapest, Hungary) 1, 217
Putsay, M. (Budapest, Hungary) 205
Radriamampianina, R. (Budapest, Hungary) 143
Robaa, S. M. (Giza, Egypt) 123
Sharov, V. (Sofia, Bulgaria) 55
Steib, R. (Budapest, Hungary) 157
Szász, G. (Debrecen, Hungary) 71
Szepesi, D. (Budapest, Hungary) 257
Szonda, S. (Budapest, Hungary) 111
Wantuch, F. (Budapest, Hungary) 111
Zsótér, E. (Budapest, Hungary) 89

TABLE OF CONTENTS

I. Papers

Alexandru, S. and *Horányi, A.:* An evaluation of the performance of the three-dimensional variational data assimilation scheme for the ALADIN/HU spectral limited area model 233

Anda, A. and *Lőke, Zs.:* Microclimate simulation in maize with two watering levels 21

Ács, F., Szász, G. and *Drucza, M.:* Estimating soil moisture content of a grass-covered surface using an energy balance approach and agroclimatological observations 71

Bartholy, J. and *Pongrácz, R.:* Tendencies of extreme climate indices based on daily precipitation in the Carpathian Basin for the 20th century 1

Cseh, S. and *Bencze, P.:* Long-term variations of temperature, wind, and precipitable water in the troposphere and lower stratosphere over Budapest, Hungary 189

Dezső, Zs., Bartholy, J. and *Pongrácz, R.:* Satellite-based analysis of the urban heat island effect 217

Hukár, M.: On the use of standard meteorological data for microclimate simulation 39

Kerényi, J. and *Putsay, M.:* Extreme flood monitoring in Romania and Hungary using Earth Observation Data 205

Ladics, T.: Analysis of the splitting error for advection-reaction problems in air pollution models 173

Marinova, T., Bocheva, L. and *Sharov, V.:* On some climatic changes in the circulation over the Mediterranean area 55

Radriamampianina, R.: Radiance-bias correction for a limited area model 143

Robaa, S. M.: A study of ultraviolet solar radiation at Cairo urban area, Egypt ... 123

Steib, R. and *Labancz, K.:* Regulatory modeling in Hungary – the AERMOD model. Part I. Description and application 157

Szepesi, D., Fekete, K., Büki, R., Koncsos, L., and *Kovács, E.:* Development of regulatory transmission modeling in Hungary 257

Wantuch, F. and *Szonda, S.:* General characterization of the lightnings in the Carpathian Basin 111

Zsótér, E.: Downscaling EPS probabilities using SYNOP precipitation data 89

II. Book review

Gelencsér, A.: Carbonaceous Aerosol (*E. Mészáros*) 139
Holton, J. R. (editor-in Chief): Encyclopedia of Atmospheric Sciences (*Gy. Gyuró*) 281
Hughton, J.: The Physics of Atmospheres (*Gy. Gyuró*) 203
Pap, J. M. and *Fox, P.* (eds.): Solar Variability and Its Effects on Climate (*G. Major*) 69
Zdunkowski, W. and *Bott, A.:* Dynamics of the Atmosphere. A Course in Theoretical Meteorology (*Gy. Gyuró*) 141
Zdunkowski, W. and *Bott, A.:* Thermodynamics of the Atmosphere. A Course in Theoretical Meteorology (*Gy. Gyuró*) .. 141

SUBJECT INDEX

A

aerosol 139
agglomeration 217
agrometeorological station 71
air pollution
- modeling 157, 173, 257
- limit values 257
atmospheres, physics of 203
atmospheric sciences 283

B

Brier score 89
boundary layer 157
Budapest agglomeration 217
Bulgaria 55

C

canopy characteristics 39
carbonaceous aerosol 139
Carpathian Basin 1
chemical reactions 173
climate 69
climate index 1
complex terrain 157
concentration
- most probable 257
- sector average 257
condensation nuclei 139
crop
- microclimate 21
- water stress index (CWSI) 21
cyclone
- activity 55
- frequency 55
- paths 55

D

data assimilation 143
- variational 233
dividing streamline height 157
dispersion modeling 157
distribution, bi-Gaussian 157
dust 123

E

Egypt 123
electrical parameters 111
elevated terrain 157
encyclopedia, atmospheric sciences 283
energy balance equation 71
ensemble forecast 89
error, splitting 173
Europe 1
extremes 1

F

flood
- management 205
- detecting 205

G

global solar radiation 123
Goudriaan
- crop microclimate simulation model 21
grass-covered surface 71

H

heat island, urban 217
Hungarian large cities 217
Hungary 21, 39, 71, 89, 111, 157, 189, 205, 217, 257

I

industrialization 123
interferometria 111
irrigation 21

L

land use map 205
lightning
- cloud-to-ground 111
- detection system SAFIR 111
- intra-cloud 111
limit values, air pollution 257
local-scale dispersion model 157
long-term changes of meteorological parameters 189

M

macrosynoptic situations 257
maize 21, 39
Mediterranean cyclones 55
microclimate maize 21, 39
model
- limited area 143
- mesoscale limited area 233
- numerical solution 173
- radiance-bias correction 143
- regulatory dispersion model 157, 257
Molenkampf-Crowley advection 173
movement of cyclones 55

O

operation splitting 173

P

path of cyclones 55
physics of atmospheres 203
planetary boundary layer 157
precipitable water 189
precipitation
- daily 1
- extreme indices 1
- probability forecast 89
- SYNOP data 89
prediction
- ensemble system 89
- verification 89
probability
- distribution function 89
- downscaling 89

R

radiance-bias correction 143
regulatory dispersion modeling 157, 257
relative operating characteristics 89
remote sensing 143, 205, 217
representativity
- error 89
- of meteorological data 257
Romania 205
roughness length 39
rural areas 123

S

SAFIR lightning detection system 111
satellite
- ATOVS/AMSU-A 143, 205
- imagery 217
- sensor MODIS 205, 217
simulation model
- of microclimate 21, 39
soil moisture 71
solar radiation
- global 123
- ultraviolet 123
solar variability 69
splitting error 173
stability categories 257
standard meteorological data 39
surface
- roughness length 39
- soil moisture content 71

T

tendency analysis 1
temperature
- long-term variation 189
- surface 217
terrain height scale 157
transmission 257
troposphere
- temperature 189
- precipitable water 189
- warming 189

U

ultraviolet solar radiation 123
urban heat island effect 217
urbanization 123

V

3D-VAR 233
variational data assimilation 233

W

warming of the atmosphere 189
water-soluble organic species 139
weather prediction, numerical 233
wind, long-term variation 189

Z

zero-plane displacement 39

GUIDE FOR AUTHORS OF *IDŐJÁRÁS*

The purpose of the journal is to publish papers in any field of meteorology and atmosphere related scientific areas. These may be

- research papers on new results of scientific investigations,
- critical review articles summarizing the current state of art of a certain topic,
- short contributions dealing with a particular question.

Some issues contain "News" and "Book review", therefore, such contributions are also welcome. The papers must be in American English and should be checked by a native speaker if necessary.

Authors are requested to send their manuscripts to

Editor-in Chief of IDŐJÁRÁS
P.O. Box 39, H-1675 Budapest, Hungary

in three identical printed copies including all illustrations. Papers will then be reviewed normally by two independent referees, who remain unidentified for the author(s). The Editor-in-Chief will inform the author(s) whether or not the paper is acceptable for publication, and what modifications, if any, are necessary.

Please, follow the order given below when typing manuscripts.

Title part: should consist of the title, the name(s) of the author(s), their affiliation(s) including full postal and E-mail address(es). In case of more than one author, the corresponding author must be identified.

Abstract: should contain the purpose, the applied data and methods as well as the basic conclusion(s) of the paper.

Key-words: must be included (from 5 to 10) to help to classify the topic.

Text: has to be typed in double spacing with wide margins on one side of an A4 size white paper. Use of S.I. units are expected, and the use of negative exponent is preferred to fractional sign. Mathematical formulae are expected to be as simple as possible and numbered in parentheses at the right margin.

All publications cited in the text should be presented in a *list of references*, arranged in alphabetical order. For an article: name(s) of author(s) in Italics, year, title of article, name of journal, volume, number (the latter two in Italics) and pages. E.g., *Nathan, K.K.*, 1986: A note on the relationship between photo-synthetically active radiation and cloud amount. *Időjárás 90,* 10-13. For a book: name(s) of author(s), year, title of the book (all in Italics except the year), publisher and place of publication. E.g., *Junge, C. E.*, 1963: *Air Chemistry and Radioactivity*. Academic Press, New York and London. Reference in the text should contain the name(s) of the author(s) in Italics and year of publication. E.g., in the case of one author: *Miller* (1989); in the case of two authors: *Gamov* and *Cleveland* (1973); and if there are more than two authors: *Smith et al.* (1990). If the name of the author cannot be fitted into the text: *(Miller,* 1989); etc. When referring papers published in the same year by the same author, letters a, b, c, etc. should follow the year of publication.

Tables should be marked by Arabic numbers and printed in separate sheets with their numbers and legends given below them. Avoid too lengthy or complicated tables, or tables duplicating results given in other form in the manuscript (e.g., graphs)

Figures should also be marked with Arabic numbers and printed in black and white in camera-ready form in separate sheets with their numbers and captions given below them. Good quality laser printings are preferred.

The text should be submitted both in manuscript and in electronic form, the latter on diskette or in E-mail. Use standard 3.5" MS-DOS formatted diskette or CD for this purpose. MS Word format is preferred.

Reprints: authors receive 30 reprints free of charge. Additional reprints may be ordered at the authors' expense when sending back the proofs to the Editorial Office.

More information for authors is available: antal.e@met.hu

Information on the last issues: http://omsz.met.hu/irodalom/firat_ido/ido_hu.html

Published by the Hungarian Meteorological Service

Budapest, Hungary

INDEX: 26 361

HU ISSN 0324-6329